The Cryosphere, 12, 1433–1460, 2018
https://doi.org/10.5194/tc-12-1433-2018

The Cryosphere Open Access EGU

Design and results of the ice sheet model initialisation experiments initMIP-Greenland: an ISMIP6 intercomparison

Heiko Goelzer[1,2], Sophie Nowicki[3], Tamsin Edwards[4,a], Matthew Beckley[3], Ayako Abe-Ouchi[5], Andy Aschwanden[6], Reinhard Calov[7], Olivier Gagliardini[8], Fabien Gillet-Chaulet[8], Nicholas R. Golledge[9], Jonathan Gregory[10,11], Ralf Greve[12], Angelika Humbert[13,14], Philippe Huybrechts[15], Joseph H. Kennedy[16,17], Eric Larour[18], William H. Lipscomb[19,20], Sébastien Le clec'h[21], Victoria Lee[22], Mathieu Morlighem[23], Frank Pattyn[2], Antony J. Payne[22], Christian Rodehacke[24,13], Martin Rückamp[13], Fuyuki Saito[25], Nicole Schlegel[18], Helene Seroussi[18], Andrew Shepherd[26], Sainan Sun[2], Roderik van de Wal[1], and Florian A. Ziemen[27]

[1]Utrecht University, Institute for Marine and Atmospheric Research (IMAU), Utrecht, the Netherlands
[2]Laboratoire de Glaciologie, Université Libre de Bruxelles, Brussels, Belgium
[3]NASA GSFC, Cryospheric Sciences Branch, Greenbelt, USA
[4]School of Environment, Earth & Ecosystem Sciences, The Open University, Milton Keynes, UK
[5]Atmosphere Ocean Research Institute, University of Tokyo, Kashiwa, Japan
[6]Geophysical Institute, University of Alaska Fairbanks, Fairbanks, USA
[7]Potsdam Institute for Climate Impact Research, Potsdam, Germany
[8]Univ. Grenoble Alpes, CNRS, IRD, Grenoble INP, IGE, 38000 Grenoble, France
[9]Antarctic Research Centre, Victoria University of Wellington, Wellington, New Zealand
[10]Department of Meteorology, University of Reading, Reading, UK
[11]Met Office Hadley Centre, Exeter, UK
[12]Institute of Low Temperature Science, Hokkaido University, Sapporo, Japan
[13]Alfred Wegener Institute for Polar and Marine Research, Bremerhaven, Germany
[14]University of Bremen, Bremen, Germany
[15]Vrije Universiteit Brussel, Brussels, Belgium
[16]Climate Change Science Institute, Oak Ridge National Laboratory, Oak Ridge, USA
[17]Computational Sciences and Engineering Division, Oak Ridge National Laboratory, Oak Ridge, USA
[18]Jet Propulsion Laboratory, California Institute of Technology, Pasadena, USA
[19]Los Alamos National Laboratory, Los Alamos, USA
[20]National Center for Atmospheric Research, Boulder, USA
[21]LSCE/IPSL, Laboratoire des Sciences du Climat et de l'Environnement, CEA-CNRS-UVSQ, Gif-sur-Yvette, France
[22]University of Bristol, Bristol, UK
[23]University of California Irvine, Irvine, USA
[24]Danish Meteorological Institute, Copenhagen, Denmark
[25]Japan Agency for Marine-Earth Science and Technology, Yokohama, Japan
[26]School of Earth and Environment, University of Leeds, Leeds, UK
[27]Max Planck Institute for Meteorology, Hamburg, Germany
[a]now at: King's College London, Department of Geography, London, UK

Correspondence: Heiko Goelzer (h.goelzer@uu.nl)

Received: 3 July 2017 – Discussion started: 14 July 2017
Revised: 9 October 2017 – Accepted: 6 February 2018 – Published: 19 April 2018

Published by Copernicus Publications on behalf of the European Geosciences Union.

Abstract. Earlier large-scale Greenland ice sheet sea-level projections (e.g. those run during the ice2sea and SeaRISE initiatives) have shown that ice sheet initial conditions have a large effect on the projections and give rise to important uncertainties. The goal of this initMIP-Greenland intercomparison exercise is to compare, evaluate, and improve the initialisation techniques used in the ice sheet modelling community and to estimate the associated uncertainties in modelled mass changes. initMIP-Greenland is the first in a series of ice sheet model intercomparison activities within ISMIP6 (the Ice Sheet Model Intercomparison Project for CMIP6), which is the primary activity within the Coupled Model Intercomparison Project Phase 6 (CMIP6) focusing on the ice sheets. Two experiments for the large-scale Greenland ice sheet have been designed to allow intercomparison between participating models of (1) the initial present-day state of the ice sheet and (2) the response in two idealised forward experiments. The forward experiments serve to evaluate the initialisation in terms of model drift (forward run without additional forcing) and in response to a large perturbation (prescribed surface mass balance anomaly); they should not be interpreted as sea-level projections. We present and discuss results that highlight the diversity of data sets, boundary conditions, and initialisation techniques used in the community to generate initial states of the Greenland ice sheet. We find good agreement across the ensemble for the dynamic response to surface mass balance changes in areas where the simulated ice sheets overlap but differences arising from the initial size of the ice sheet. The model drift in the control experiment is reduced for models that participated in earlier intercomparison exercises.

1 Introduction

Ice sheet model intercomparison exercises have a long history, going back to the advent of large-scale ice sheet models in the early 1990s. The first intercomparison project (EISMINT, the European Ice Sheet Modelling INiTiative; Huybrechts et al., 1996) defined three levels of possible comparisons that could be distinguished. EISMINT and later following comparisons include (1) schematic experiments with identical model setup and boundary conditions between models (e.g. Huybrechts et al., 1996; Pattyn et al., 2008, 2012, 2013), (2) experiments allowing individual modelling decisions (e.g. Payne et al., 2000; Calov et al., 2010; Asay-Davis et al., 2016), and (3) experiments of models applied to real ice sheets (e.g. Shannon et al., 2013; Edwards et al., 2014b; Bindschadler et al., 2013; Nowicki et al., 2013a, b). In this genealogy, the present intercomparison is a type 3 experiment with ice sheets models applied to simulate the large-scale present-day Greenland ice sheet (GrIS). The role of this study is to assess the impact of initialisation on model behaviour; it is a precursor to ice sheet mass budget projections made using climate forcing for the atmosphere and ocean. The initMIP-Greenland project is the first intercomparison within ISMIP6, the Ice Sheet Model Intercomparison Project for CMIP6 (Nowicki et al., 2016), which is the primary activity within the Coupled Model Intercomparison Project Phase 6 (CMIP6, Eyring et al., 2016) focusing on the ice sheets. ISMIP6 is the first ice sheet model intercomparison that is fully integrated within CMIP. This is an improvement to earlier initiatives like ice2sea (Gillet-Chaulet et al., 2012; Shannon et al., 2013; Goelzer et al., 2013; Edwards et al., 2014a, b) and SeaRISE (Sea-level Response to Ice Sheet Evolution; Bindschadler et al., 2013; Nowicki et al., 2013a, b), which were lagging one iteration behind in terms of applied climate forcing. More information on ISMIP6 can be found in the description paper (Nowicki et al., 2016) and on the Climate and Cryosphere (CliC)-hosted webpage (http://www.climate-cryosphere.org/activities/targeted/ismip6).

The initialisation of an ice sheet model forms the basis for any prognostic model simulation and therefore reveals most of the modelling decisions that distinguish different approaches (Goelzer et al., 2017). It consists of defining both the initial physical state of the ice sheet and model parameter values. In the context of initMIP-Greenland, we focus on initialisation to the present day as a starting point for centennial timescale future-sea-level-change projections (Nowicki et al., 2016). The need for physical ice flow models for such projections lies in the dynamic and highly non-linear response of ice sheet flow to changes in climatic forcing at the atmospheric and oceanic boundaries. The surface mass balance (SMB) of the ice sheet is governed by the amount of precipitation falling on the surface and by meltwater runoff removing mass predominantly at the margins. Mass is also lost by melting at surfaces in contact with ocean water and by calving of icebergs from marine-terminating outlet glaciers. Changes in ice sheet geometry generally cause changes in atmospheric conditions over the ice sheet and hence changes in SMB. An important effect is the height–SMB feedback, which causes decreasing SMB with decreasing ice surface elevation and vice versa (e.g. Helsen et al., 2012; Franco et al., 2012; Edwards et al., 2014a; b). An important consequence of the relation between SMB and ice flow is that negative SMB removes ice before it can reach the marine margins and thereby reduces the calving flux (e.g. Gillet-Chaulet et al., 2012; Goelzer et al., 2013; Fürst et al., 2015). An estimate for the recent balance of processes indicates that ablation (i.e. negative SMB) is responsible for two-thirds of the increasing GrIS mass loss in the period 2009–2012, with ice discharge from marine-terminating outlet glaciers accounting for the remaining third (Enderlin et al., 2014). While the relative importance of outlet glacier dynamics for total GrIS mass loss has decreased since 2001 (Enderlin et al., 2014) and is expected to decrease further in the future (e.g. Goelzer et al., 2013; Fürst et al., 2015), it remains an important aspect for projecting future sea-level contributions from the ice sheet on the centennial timescale.

Observations of ice sheet geometry and surface velocity, which ultimately form the target for any initialisation to the present-day state, have existed for only ~ 25 years, i.e. only since the advent of the satellite era (e.g. Mouginot et al., 2015). This is a short period compared to the longer response times of the ice sheet, which can be up to several thousand years (Drewry et al., 1992), and makes it impossible to understand ice sheet changes based on observations alone. While detailed observations mainly cover the ice surface properties, measurements for the ice interior and bed conditions are limited to a handful of deep ice core drilling sites. Radar layers dated at ice core sites can be used to extend the dating over large parts of the Greenland ice sheet (MacGregor et al., 2015), but this information is not well explored by ice sheet modellers so far.

Projections of ice sheet response on decadal to centennial timescales are strongly influenced by the initial state of the ice sheet model (e.g. Arthern and Gudmundsson, 2010; Nowicki et al., 2013b; Adalgeirsdottir et al., 2014; Saito et al., 2016). The prognostic variables and parameters that need to be defined for the initial state of an ice sheet model at the present day depend to some extent on the complexity of the modelling approach but typically consist of ice temperature (due to its impact on both ice rheology and basal slip), ice sheet geometry, and boundary conditions at the base of the ice sheet. For this time frame, ice sheet modellers face an issue similar to the one encountered in the weather/climate community: whether to treat the problem as a "boundary value problem" (climate prediction) or as an "initial-value problem" (weather forecasting).

Models developed for long-term and palaeoclimate simulations typically use "spin-up" procedures to determine the initial state, where the ice sheet model is run forward in time for tens to hundreds of thousands of years with (changing) reconstructed or modelled climatic boundary conditions (e.g. Huybrechts and de Wolde, 1999; Greve et al., 2011; Aschwanden et al., 2013). This implies that at any time during the simulation (except at the beginning where arbitrary conditions are set) the model's state is defined as a consistent response to the forcing. Imperfections due to applied physical approximations, limited spatial resolution, and uncertainty in physical parameters and climatic boundary conditions can result in a considerable mismatch between the spun-up state and present-day observations.

The main alternative to the spin-up approach is to use data assimilation techniques, which leverage high-resolution observations of geometry and velocity to initialise ice sheet models to the present-day state (e.g. Gillet-Chaulet et al., 2012; Seroussi et al., 2013; Arthern et al., 2015). They typically infer poorly constrained basal conditions by a formal partial-differential-equations-constrained optimisation to match observed surface velocities for a given geometry (e.g. Morlighem et al., 2010). This implies that the inferred basal parameters remain constant throughout the simulation, which is limited to the centennial timescale, where this is approximately the case. Data assimilation techniques produce an initial state as consistent as possible with observational data but are affected by inconsistences (e.g. ice temperature not in equilibrium with the stress regime) and by uncertainties in observations (e.g. inconsistencies between different observational data sets; Seroussi et al., 2011). As data assimilations are designed to best fit observations, errors arising from choices in ice parameters, from physical processes, from model resolution, from observational data sets, or from ignoring relevant state variables (e.g. ice rheology) are transferred to basal conditions or other parameters obtained by inversion. An intermediate approach is assimilation of the geometry of the ice sheet, by finding basal conditions that reduce the mismatch with the observed ice sheet surface (Pollard and DeConto, 2012b). This method is typically applied during forward integration of the model and implies a model state in near balance with the forcing, though with a degree of compromise over matching observations. Note that the division of the different initialisation approaches presented here is somewhat arbitrary. Combinations between different approaches (e.g. relaxation after data assimilation) exist and need to be further explored to improve initialisation techniques in the future.

Given the wide diversity of ice sheet initialisation techniques, the goal of initMIP-Greenland is to document, compare, and improve the techniques used by different groups to initialise their state-of-the-art whole-ice-sheet models to the present day as a starting point for centennial-timescale future-sea-level-change projections. A related goal is to highlight and understand how much of the spread in simulated ice sheet evolution is related to the choices made in the initialisation. All three methods currently used for initialisation of ice sheet models (spin-up, assimilation of velocity, and assimilation of surface elevation) and variations thereof are represented in our ensemble. We first describe our approach and experimental setup in Sect. 2, and we present the participating models in Sect. 3. Section 4 concentrates on the results, with the ice sheet model initial state explored in Sect. 4.1 and the impact of initialisation on ice sheet evolutions analysed in Sect. 4.2. Discussion and conclusions follow in Sect. 5.

2 Approach and experimental setup

In initMIP-Greenland we focus on stand-alone ice sheet models, i.e. models not coupled to climate models. Although some participating models have the capability to produce their own SMB forcing, this is not a requirement in the present study. We have chosen to leave most of the modelling decisions to the discretion of the participants, which serves to document the current state of the initialisation techniques used in the ice sheet modelling community. Conversely, this implies a relatively heterogeneous ensemble with only incidental overlap of modelling choices between different submissions.

Table 1. Summary of the ISMIP6 initMIP-Greenland experiments (n/a: not applicable).

Experiment title	Experiment label	CMIP6 Label (experiment_id)	Experiment description	Duration of the simulation	Major purposes
Initialisation	init	ism–init–std	Initialisation to present day	n/a	Evaluation
Control	ctrl	ism–ctrl–std	Unforced control experiment	100 yr	Evaluation
SMB anomaly	asmb	ism–asmb–std	Idealised change in SMB forcing	100 yr	Evaluation

Experiments for the large-scale Greenland ice sheet have been designed to allow intercomparison of the modelled initial present-day states and of the model responses to a large perturbation in SMB forcing (Table 1). Modellers were asked to initialise their model to the present day with the method of their choice (init) and then run two forward experiments to evaluate the initialisation in terms of model drift: a control run without any change in the forcing (ctrl) and a perturbed run with a large prescribed surface mass balance anomaly (asmb). The prescribed SMB anomaly in experiment asmb (Appendix A) implies a strongly negative SMB forcing, in line with what may be expected from upper-end climate change scenarios. Nevertheless, the sea-level contribution from these experiments should not be interpreted as a projection, but rather as a diagnostic to evaluate model differences.

Note that the time of initialisation was not strictly defined (in the range 1950–2016), as modellers assign different dates to their initial state according to the data sets used. The participants were also largely free in other modelling decisions, with only the imposed constraint for the forward experiments that all boundary conditions and forcing remain constant in time. In particular, the SMB is not allowed to change (e.g. with surface elevation) other than by the prescribed SMB anomaly. All information and documentation concerning the ISMIP6 initMIP-Greenland experiments can be found on the ISMIP6 wiki (http://www.climate-cryosphere.org/wiki/index.php?title=InitMIP-Greenland).

While modellers were free to use a native model grid of their choice, model output was submitted on a common grid to support a consistent analysis (see Appendix C). This implies that results had to first be interpolated from the native model grid to the output grid, which for state variables has in most cases been done using conservative interpolation (Jones, 1999). In the following we present all results on the output grid with a horizontal resolution of 5×5 km. Furthermore, all ice sheet results have been masked to exclude ice on Ellesmere Island and Iceland.

3 Participating groups and models

Participants in initMIP-Greenland from 17 groups and collaborations (Table 2) have provided 35 model submissions. There is some overlap between the code bases used by different groups, with ultimately 11 individual ice flow models. However, the same model used by different groups (with varying data sets and initialisation procedures) may lead to rather different results. These submissions cover a wide spectrum of model resolutions, applied physical approximations, boundary conditions, and initialisation techniques, which makes for a heterogeneous ensemble. In some cases, the same group has used two or more different model versions or different initialisation techniques, with several groups running their models at varying horizontal grid resolution. In the following we will refer to each separate submission as a "model", identified by the model ID in the table of general model characteristics (Table 3). A detailed description of the individual models and initialisation techniques can be found in Appendix B.

Despite the diversity in modelling approaches (Table 3) and the overlap between different methods, it is useful to distinguish the three main classes of initialisation techniques described before: first, those using a form of data assimilation (DA) to match observed velocities (DAv); second, those that rely solely on model spin-up (SP); and third, the intermediate case of transient assimilation to match surface elevation (DAs). However, even DAv is typically preceded by some form of spin-up (with the same model or a different one) to produce the internal temperature of the ice sheet, and it may also be followed by a relaxation run to make the velocities and geometry more consistent. The represented cases of DA infer a spatially varying basal drag coefficient to minimise the mismatch with observations of velocity or geometry. Models using SP use physical parameters and processes to define the basal conditions.

Modelling choices also differ based on model purpose and typical application. Many of the SP models have been built and used for palaeo-applications for time periods when possible DA targets are very limited and SMB boundary conditions differ from the present. This makes it necessary in those models to parameterise SMB, for example by using positive-degree-day (PDD) models (e.g. Huybrechts et al., 1991). SP approaches are also generally favoured when including ice sheets in coupled climate models. In two groups (DMI, MPIM), the ice sheet models and SMB forcing are set up in a similar way to how they would be for coupled ice sheet–climate simulations. In contrast, the DAv models are built specifically for centennial timescale future projections, while DAs again represents an intermediate case of models typically used for long-term simulations but specifically initialised for the present day. These fundamental differences in modelling approaches have to be kept in mind when comparing the models. The SMB is in many cases taken from

Table 2. Participants, ice sheet models, and modelling groups in ISMIP6 initMIP-Greenland.

Contributors	Model	Group ID	Group
Victoria Lee, Stephen L. Cornford, Antony J. Payne, Daniel F. Martin	BISICLES	BGC	Centre for Polar Observation and Modelling, School of Geographical Sciences, University of Bristol, Bristol, UK; Department of Geography, College of Science, Swansea University, Swansea, UK; Computational Research Division, Lawrence Berkeley National Laboratory, Berkeley, California, USA
William H. Lipscomb, Joseph H. Kennedy	CISM	LANL	Los Alamos National Laboratory, Los Alamos, USA; National Center for Atmospheric Research, Boulder, USA; Climate Change Science Institute, Oak Ridge National Laboratory, Oak Ridge, USA; Computational Sciences and Engineering Division, Oak Ridge National Laboratory, Oak Ridge, USA
Fabien Gillet-Chaulet, Olivier Gagliardini	Elmer	IGE	Institut des Géosciences de L'Environnement, Univ. Grenoble Alpes, CNRS, IRD, Grenoble INP, IGE, 38000 Grenoble, FR
Sainan Sun, Frank Pattyn	FETISH	ULB	Laboratoire de Glaciologie, Université Libre de Bruxelles, Brussels, BE
Philippe Huybrechts, Heiko Goelzer	GISM	VUB	Vrije Universiteit Brussel, Brussels, BE
Sébastien Le clec'h	GRISLI	LSCE	LSCE/IPSL, Laboratoire des Sciences du Climat et de l'Environnement, CEA-CNRS-UVSQ, Gif-sur-Yvette, FR
Fuyuki Saito, Ayako Abe-Ouchi	IcIES	MIROC	Japan Agency for Marine-Earth Science and Technology, JP; The University of Tokyo, Tokyo, JP
Heiko Goelzer, Roderik van de Wal	IMAUICE	IMAU	Utrecht University, Institute for Marine and Atmospheric Research (IMAU), Utrecht, NL
Helene Seroussi, Nicole Schlegel	ISSM	JPL	Caltech's Jet Propulsion Laboratory, Pasadena, USA
Helene Seroussi, Mathieu Morlighem	ISSM	UCI_JPL	Caltech's Jet Propulsion Laboratory, Pasadena, USA; University of California Irvine, USA
Martin Rückamp, Angelika Humbert	ISSM	AWI	Alfred Wegener Institute for Polar and Marine Research, DE; University of Bremen, DE
Andy Aschwanden	PISM	UAF	Geophysical Institute, University of Alaska Fairbanks, USA
Nicholas R. Golledge	PISM	ARC	Antarctic Research Centre, Victoria University of Wellington, NZ
Christian Rodehacke	PISM	DMI	Danish Meteorological Institute, DK; Alfred Wegener Institute for Polar and Marine Research, DE
Florian A. Ziemen	PISM	MPIM	Max Planck Institute for Meteorology, DE
Ralf Greve	SICOPOLIS	ILTS	Institute of Low Temperature Science, Hokkaido University, Sapporo, JP
Ralf Greve, Reinhard Calov	SICOPOLIS	ILTS_ PIK	Institute of Low Temperature Science, Hokkaido University, Sapporo, JP; Potsdam Institute for Climate Impact Research, Potsdam, DE

regional climate model (RCM) simulations, but it arises in some cases from parameterisations based on the modelled ice sheet geometry applying traditional PDD methods.

4 Results

In this section, we first present results of the init experiment, designed to compare the present-day initial state between participating models and against observations. These or similar initial model states would serve as a starting point for physically based projections of the Greenland ice sheet con-

Table 3. Model characteristics. Model ID: cf. Table 2. Numerical method: FD – finite difference; FE – finite element; FV – finite volume with adaptive mesh refinement. Ice flow: SIA – shallow-ice approximation; SSA – shallow-shelf approximation; HO – higher order; HYB – SIA and SSA combined. Initialisation method: DAv – data assimilation of velocity; DAs – data assimilation of surface elevation; SP – spin-up. Initial SMB: RA1 – RACMO2.1; RA3 – RACMO2.3; HIR – HIRHAM5; MAR – MAR; BOX – BOX reconstruction (synthesis of simulation and data); PDD – positive-degree-day model; EBM – energy balance model (EBM). Velocity: RM – Rignot and Mouginot; J – Joughin et al. Bed and surface: M – Morlighem et al.; B – Bamber et al.; H – Herzfeld et al. Geothermal heat flux (GHF): SR – Shapiro and Ritzwoller; G – Greve; P – Purucker; FM – Fox Maule et al. CST – constant. Model resolution (Res) in kilometres. In the case of heterogeneous grid resolution, the minimum and maximum resolution are given.

Model ID	Numerics	Ice flow	Initialisation	Initial year(s)	Initial SMB	Velocity	Bed	Surface	GHF	Res min	Res max
ARC-PISM	FD	HYB	SP	2000	RA1		B		SR	5	5
AWI-ISSM1[a]	FE	HO	DAv	2000	RA3	RM	M		SR	2.5	35
AWI-ISSM2[a]	FE	HO	DAv	2000	RA3	RM	M		SR	2.5	35
BGC-BISICLES1	FV	SSA	DAv	1997–2006	HIR	RM	M			1.2	4.8
BGC-BISICLES2	FV	SSA	DAv	1997–2006	HIR	RM	M			2.4	4.8
BGC-BISICLES3	FV	SSA	DAv	1997–2006	HIR	RM	M			4.8	4.8
DMI-PISM1[b]	FD	HYB	SP	2000	PDD		B		SR	5	5
DMI-PISM2[b]	FD	HYB	SP	2000	PDD		B		SR	5	5
DMI-PISM3[b]	FD	HYB	SP	2000	PDD		B		SR	5	5
DMI-PISM4[b]	FD	HYB	SP	2000	PDD		B		SR	5	5
DMI-PISM5[b]	FD	HYB	SP	2000	PDD		B		SR	5	5
IGE-ELMER1	FE	SSA	DAv	2000–2010	MAR	J	M			1.5	45
IGE-ELMER2	FE	SSA	DAv	2000–2010	MAR	J	M			1	5
ILTS-SICOPOLIS	FD	SIA	SP	1990	PDD		B		P	5	5
ILTSPIK-SICOPOLIS	FD	SIA	SP	1990	PDD		H		G	5	5
IMAU-IMAUICE1	FD	SIA	SP	1990	RA3		B		SR	5	5
IMAU-IMAUICE2	FD	SIA	SP	1990	RA3		B		SR	10	10
IMAU-IMAUICE3	FD	SIA	SP	1990	RA3		B		SR	20	20
JPL-ISSM	FE	SSA	DAv	2012	BOX	RM	M		SR	1	15
LANL-CISM	FE	HO	SP	1961–1990	RA1		M		CST	4	4
LSCE-GRISLI	FD	HYB	DAv	2000	MAR	J	B		FM	5	5
MIROC-ICIES1	FD	SIA	DAs	2004	RA1		B	B	SR	10	10
MIROC-ICIES2	FD	SIA	SP	2004	PDD		B		SR	10	10
MPIM-PISM	FD	HYB	SP	2006	EBM		B		SR	5	5
UAF-PISM1[c]	FD	HYB	SP	2007	RA1		M		SR	1.5	1.5
UAF-PISM2[c]	FD	HYB	SP	2007	RA1		M		SR	3	3
UAF-PISM3[c]	FD	HYB	SP	2007	RA1		M		SR	4.5	4.5
UAF-PISM4[c]	FD	HYB	SP	2007	RA1		M		SR	1.5	1.5
UAF-PISM5[c]	FD	HYB	SP	2007	RA1		M		SR	3	3
UAF-PISM6[c]	FD	HYB	SP	2007	RA1		M		SR	4.5	4.5
UCIJPL-ISSM	FE	HO	DAv	2007	RA1	RM	M		SR	0.5	30
ULB-FETISH1	FD	SIA	DAs	1979–2006	MAR		B	B	FM	10	10
ULB-FETISH2	FD	HYB	DAs	1979–2006	MAR		B	B	FM	10	10
VUB-GISM1	FD	HO	SP	2005	PDD		B		SR	5	5
VUB-GISM2	FD	SIA	SP	2005	PDD		B		SR	5	5

[a] AWI-ISSM2 differs from AWI-ISSM1 in the climatic forcing used during temperature spin-up. [b] DMI-PISM1–5 differ in the melt parameters of the PDD model. [c] UAF-PISM4–6 differ from UAF-PISM1–3 in the initial geometry.

tribution to future sea-level changes (Nowicki et al., 2016). We then present results for the two forward experiments that serve to further evaluate the response of these initial states to idealised forcing (ctrl, asmb).

4.1 Evaluation of the initial state

Because initialisation techniques generally differ in the observational data used as model input, boundary conditions, and assimilation targets, we did not prescribe the year(s) of initialisation. The initialisation times in the ensemble (Table 3) therefore represent the time frame(s) of the observations that are used for data assimilation (in case DA) and the simulated SMB used as a boundary condition for the individual models. For the comparative analysis, we did not attempt to correct the differences arising from different initialisation times. Compared to the range of modelling uncertainties, this assumption probably holds for the geometry of the ice sheet but is more questionable for velocity. However, the sparseness and limited temporal resolution of available observations preclude analysing models with respect to their individual reference time frame. Where available, we have used a range of observational data sets to compare against.

The modelled present-day ice extent (Fig. 1) exhibits a large spread among models and ranges from the extent of the observed ice sheet proper (excluding connected glaciers and ice caps) to nearly filling the entire land above sea level (see also Supplement Fig. S2 for individual model results). This

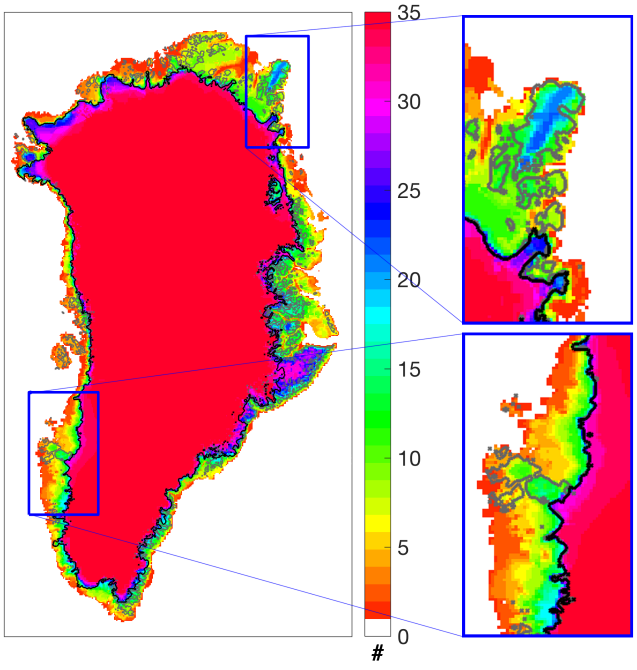

Figure 1. Common ice mask of the ensemble of models in the intercomparison. The colour code indicates the number of models (out of 35 in total) that simulate ice at a given location. Outlines of the observed ice sheet proper (Rastner et al., 2012) and all ice-covered regions (i.e. main ice sheet plus small ice caps and glaciers; Morlighem et al., 2014) are given as black and grey contour lines, respectively. A complete set of figures displaying individual model results is given in the Supplement.

diversity in the ensemble is representative of the large range of modelling choices and initialisation techniques. For example, the assumption of what should be modelled (only the ice sheet, or including outlying glaciers and ice caps) differs from group to group. Also, models may simulate ice in places where no ice is observed. While some models prescribe a fixed (observed) ice mask and prevent any ice growing outside, most models simulate ice margins that are free to evolve according to the balance of ice flow and SMB. In some cases, modellers have controlled the extent where ice sheets are allowed to grow, for example by prescribing a negative SMB over observed ice-free regions.

The diversity of modelling choices equally leads to a large spread in the simulated total ice area and volume at the present day (Fig. 2; see Supplement Table S1 for the numbers). In comparison with observations (Morlighem et al., 2014), the initial ice sheet area (horizontal axis in Fig. 2) of many models is "bracketed" by the observed extent (cf. Fig. 1) of the ice sheet proper (black diamond) and the extent of the entire ice-covered areas (grey diamond). Differences in observed volume (vertical axis in Fig. 2) between these two defined areas are small compared to the ensemble spread; i.e. the proportional change from including ice caps and glaciers surrounding the Greenland ice sheet to volume (0.3 %) is much smaller than to area (8.2 %). An alternative data set (Bamber et al., 2013) provides similar numbers for observed volume and area (not shown). Overestimation of modelled ice sheet area (by up to 15 %) is common, and overestimation of volume (up to 15 %) is more prevalent than underestimation.

As an important input for the ice sheet simulations, we evaluate the implemented SMB of the different models. Figure 3 shows the typical present-day SMB applied for three of the models spanning the distribution of ice thickness error (see below), while an overview of all models is given in Supplement Fig. S2. In the three cases shown, one model applied SMB from a RCM with no modification (AWI-ISSM2), another (MIROC-ICIES) used a PDD method, and the last (MPIM-PISM) obtained the SMB from an energy balance model (EBM) designed for coupling of the ice sheet model to a climate model.

Because we generally cannot distinguish individual accumulation and ablation processes for the SMB prescribed during initialisation, we separate the assumed SMB into negative and positive regions (i.e. ablation and accumulation zones) for further analysis. Partitioning of mass change processes between SMB and dynamic changes (e.g. van den Broeke et al., 2009; Enderlin et al., 2014) would also be an important diagnostic to analyse. However, the participating models have not incorporated the required mechanisms, and we also lack the necessary forcing, to generate fast dynamical response due to outlet glacier changes in the current experiments. Displaying the SMB magnitude for accumulation and ablation regimes allows us to identify some important outliers (Fig. 4a) and frame the model input compared to estimates of total SMB from a range of RCMs (Fig. 4b). Apparent outliers are models with small ablation zones and large positive SMB (far right in Fig. 4a) and those with a large ablation area (top in Fig. 4a). Several of the remaining models cluster around RCM estimates (van Angelen et al., 2014; Fettweis et al., 2017; Noël et al., 2016) for the SMB partitioning, again considering either all ice-covered regions or only the ice sheet proper. This is mostly the case because the models use these or similar products. However, an additional condition required for close agreement with RCM estimates is that the modelled ice sheet be close to the observed extent. Models that lie further from RCM estimates (in Fig. 4b) typically have larger ablation zones and consequently larger negative SMB.

We further evaluate the prescribed SMB in comparison to point observations (Fig. 5). Available SMB observations (Machguth et al., 2016; Bales et al., 2009) are sparse, especially in the centre of the ice sheet, and have heterogeneous temporal coverage. However, comparison against those observations allows for a first-order evaluation of the SMB inputs chosen or produced by the modellers. Overall, positive SMB is better represented in the chosen SMB data sets than negative SMB. The order-of-magnitude difference in

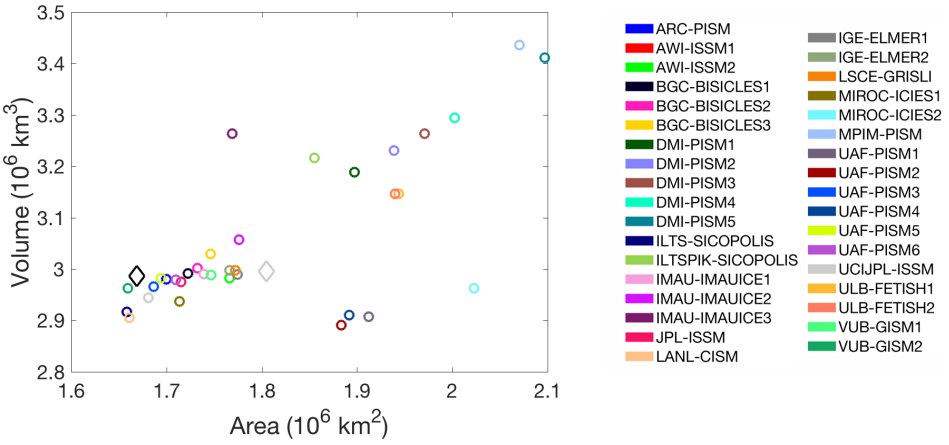

Figure 2. Grounded ice area and grounded volume for all models (circles). Observed values (Morlighem et al., 2014) are given for the entire ice-covered region (grey diamond) and for the region of the ice sheet proper (black diamond) according to the mask of Rastner et al. (2012) shown in Fig. 1.

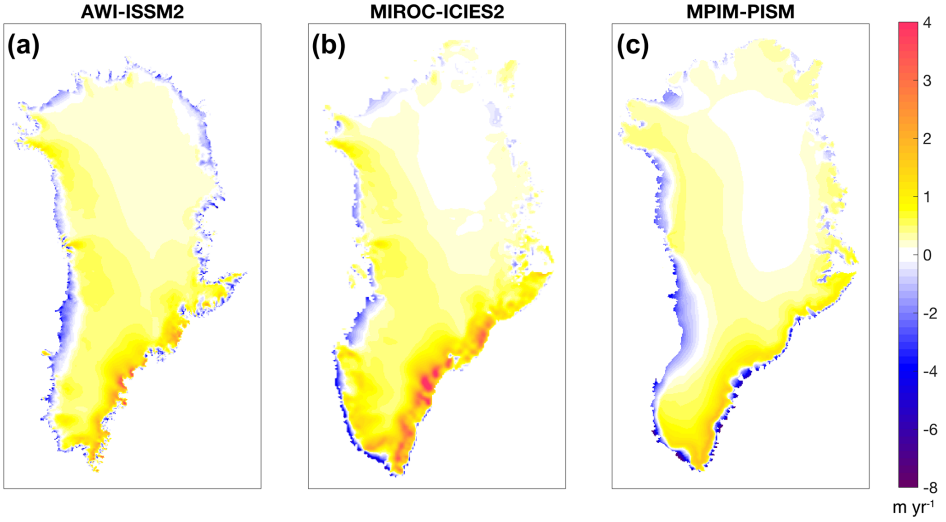

Figure 3. Typical surface mass balance for the initial state for three different models. Note the unequal scaling for positive and negative values.

root mean square error (RMSE) between the two measures is partly explained by the relatively low accumulation over a large area in the centre of the ice sheet, compared to relatively high ablation over a narrow marginal zone, which is easily misrepresented in models with too large an ice extent. While the best match with observations in both regions is produced by models using SMB derived from RCMs, good agreement with the observed SMB can also be found for some models using PDD. Again, a good match with the observed ice extent is more important than the SMB model itself to reduce the mismatch with measured SMB.

The match of the initial ice sheets with observed geometry (Morlighem et al., 2014) is evaluated as the RMSE between modelled and observed ice thickness (Fig. 6). Interpretation of the diagnostics requires distinction between the different initialisation techniques, because the geometry is a prognostic variable in some cases of SP but a given constraint during initialisation for DA. In some cases of SP, the ice sheet area is effectively confined to the observed, which represents an intermediate case. For models covering a range of horizontal resolutions, accuracy generally decreases with coarser horizontal grid resolution (BISICLES, IMAUICE, ELMER), except for UAF_PISM, where the trend is not clear. Using a different observational data set (Bamber et al., 2013) to calculate the diagnostic gives overall similar results (not shown). However, it is noticeable that DA models that have been initialised with one data set show lower errors than that specific set of observations. This point requires attention, should this diagnostic be used to formally evaluate and score the models at some stage.

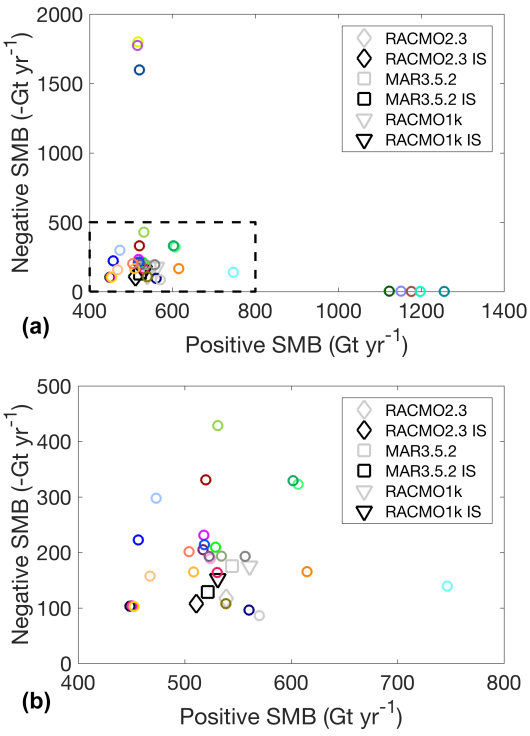

Figure 4. Negative and positive SMB of all models **(a)** and for the marked inset excluding outliers **(b)**. Diamonds, squares, and triangles in **(b)** give partitioning from average 1979–2000 regional climate model simulations (van Angelen et al., 2014; Fettweis et al., 2017; Noël et al., 2016) with masking to the ice-covered region (grey) and to the ice sheet proper (IS, black) according to the mask of Rastner et al. (2012). Compare symbol colour to identify individual models with Figs. 3–5. Data are available in Supplement Table S1.

To evaluate the match of the models with observed surface ice velocities, we have computed the RMSE between the modelled and observed (Joughin et al., 2016) velocity magnitude (Fig. 7a). Calculating the RMSE based on the log of the velocities instead (Fig. 7b) results in a slightly different picture, because errors in high velocities typically occurring at the margins over a relatively small fraction of the ice sheet area are weighted less. We note that an alternative choice of metric would be one that accounts for spatial variation in observational uncertainty, such as standardised Euclidean distance. Distinction between models using DAv and the rest is again useful, since velocity is not an independent variable in cases where it enters the inversion calculations. Models using observed velocities in the DAv procedure could in principle be compared with each other to evaluate the success of the inversion technique. However, the comparison would have to take into account that some groups use relaxation after the DAv step to get a better consistency between the ice geometry and velocity. This modifies the results depending on the relaxation time. Better consistency for a model can be achieved with longer relaxation time, at the expense of a larger discrepancy with the observed geometry. In any case, not every group uses the same velocity data set (e.g. Rignot and Mouginot, 2012; Joughin et al., 2016).

It is interesting to note that DAs techniques using only surface elevation as an inversion target can have quite low errors in simulated velocities, which implies an overall consistency between geometry and velocity structure of the modelled ice sheets. Although this consistency is expected based on mass conservation, the results confirm that the basic assumptions (e.g. approximation to the force balance and rheology structure) are generally close enough to reality. This is particularly important considering that DAv techniques can match observed velocities well for almost any given rheology, as all the uncertainty (including unknown rheology) is compounded in the basal sliding relation.

4.2 Results of the forward experiments

The two experiments ctrl and asmb have been performed to further test the modelled initial states in terms of their behaviour in typical forward simulations. This is needed to expose model response to changing constraints that were present during initialisation. Furthermore, we evaluate the influence of the initial state and of modelling decisions pertaining to the initialisation on the results of the forward experiments, i.e. the projected ice thickness change and sea-level contribution.

The experiment ctrl serves to evaluate the model response in the absence of additional forcing and is an important step to understand the consequence of modelling choices for forward experiments. Since we have not specified any assumption on the imbalance between SMB and ice flow at the initial state, the ice sheet would ideally exhibit an imbalance that matches observations for a given time interval. Recent modelled mass trends or thickness changes could then in principle be evaluated with existing observational data sets of limited time coverage (e.g. Velicogna et al., 2014). Reproducing recent changes seen by GRACE (mass change) and altimetry (thickness change), however, is hampered by not knowing the ice sheet bedrock and surface elevation well at the time that the satellite started to observe and would also assess the accuracy of the SMB input (i.e. for many models, a separate RCM). Furthermore, this would require that the experiments aimed for realistic outlet glacier dynamics and ocean forcing (e.g. Nick et al., 2013), which are currently not available (Alexander et al., 2016; Schlegel et al., 2016) and have deliberately not been included in the present experiments. Approaches to validate models using hindcasting techniques (Aschwanden et al., 2013; Larour et al., 2014, 2016; Price et al., 2017) currently suffer the same limitations of observational data sets with short time coverage, uncertainty in external forcing, limited knowledge of processes responsible for dynamic outlet glacier response, and the initialisation problems discussed above.

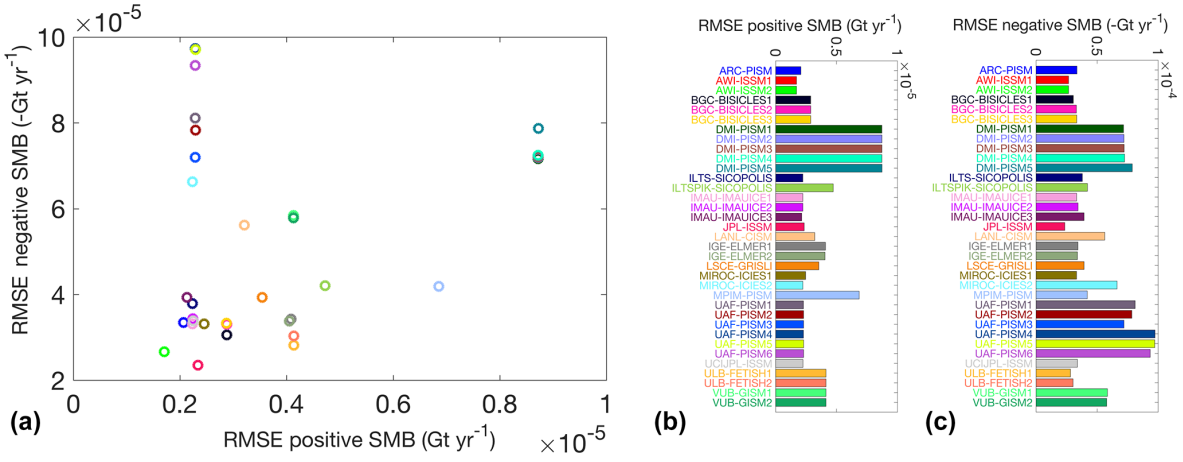

Figure 5. Root mean square error (RMSE) of initial modelled surface mass balance compared to observations for the accumulation zone (**b** and abscissa in **a**) and the ablation zone (**c** and ordinate in **a**). The observational data sets are from Bales et al. (2009) for the accumulation zone and Machguth et al. (2016) for the ablation zone.

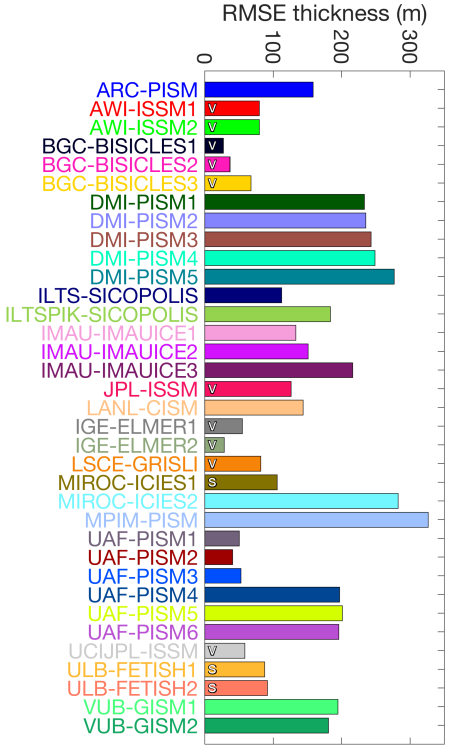

Figure 6. Root mean square error (RMSE) of initial modelled ice thickness compared to observations (Morlighem et al., 2014). The diagnostic has been calculated for subsampled data to reduce spatial correlation, and we show median values for different offsets. Letters in the bars denote assimilation targets for methods DAv and DAs and are left empty for SP.

The simulated ice mass evolution in ctrl (Fig. 8a) reflects the wide spread of initial ice mass among the models and a relatively small mass change for most of them over the course of the 100-year experiment. This is because a common approach is to attempt initialisation to a steady state with a given SMB forcing, possibly followed by relaxation or by a run with recent SMB forcing. Total mass changes in experiment ctrl (Fig. 8b) range from ~ -20 to $+25$ mm sea-level equivalent (SLE) when nine obvious outliers (discussed in context of Fig. 4) are ignored. Note that the total mass change is not a complete measure of the model drift, since positive and negative trends at different places can compensate. To calculate the SLE contribution for all models consistently, we have masked out ice outside of Greenland (Ellesmere Island and Iceland), considered only the ice mass above floatation, applied a correction to compensate for the map projection error (Snyder, 1987), and converted volume to mass using the specific ice densities from each model. In some cases of the ensemble (typically for the SP models), the modelled background trend arises from transient forcing of SMB and temperature over the past, but more often it is due to inconsistencies introduced during initialisation (i.e. the trends are dominated by the model's response to the initialisation, not to the forcing).

For DAv models (filled symbols in Fig. 8b), the mass trend in experiment ctrl represents an important diagnostic to complement the measured accuracy of matching the observed geometry, because it will also reflect any inconsistencies between ice velocity and geometry data sets (Seroussi et al., 2011). This can be illustrated by considering a forward-model run that is started from an exactly specified geometry as the initial state. Optimised model velocities combined with imperfect ice thickness reconstructions may result in a flux divergence that is unbalanced by the local SMB, which leads to large model drift. Conversely, ice sheet models can be relaxed to a steady state when constraints on the target geometry are loosened completely. Match with the observed geometry in the initial state and model drift in the forward ex-

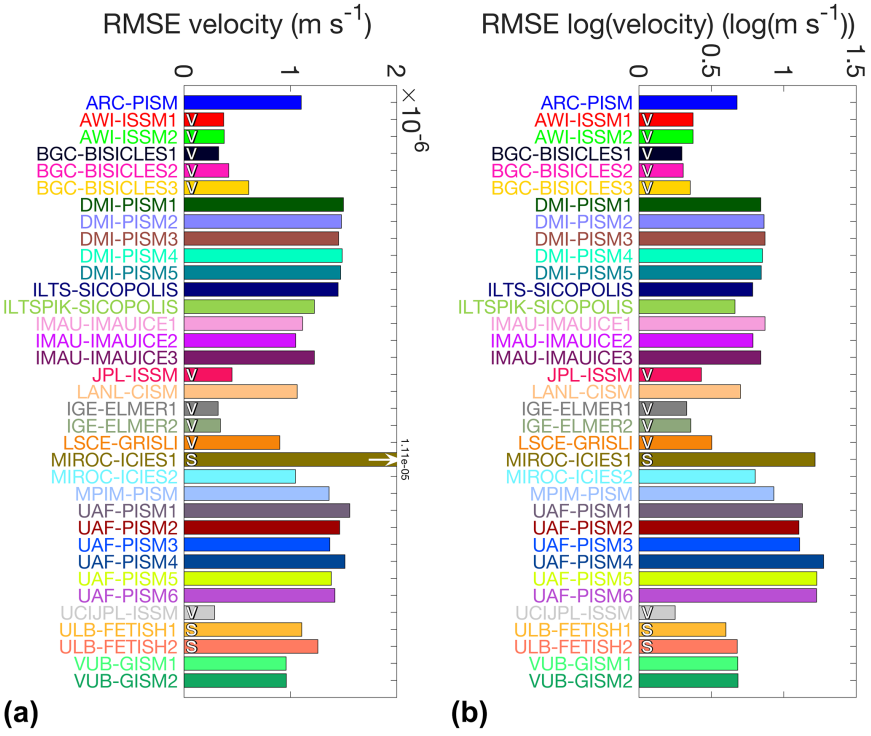

Figure 7. Root mean square error (RMSE) of the horizontal velocity magnitude **(a)** and the log of the horizontal velocity magnitude **(b)** compared to observations (Joughin et al., 2016). The diagnostics have been calculated for grid cells subsampled regularly in space to reduce spatial correlation; we show median values for different possible offsets of this sampling.

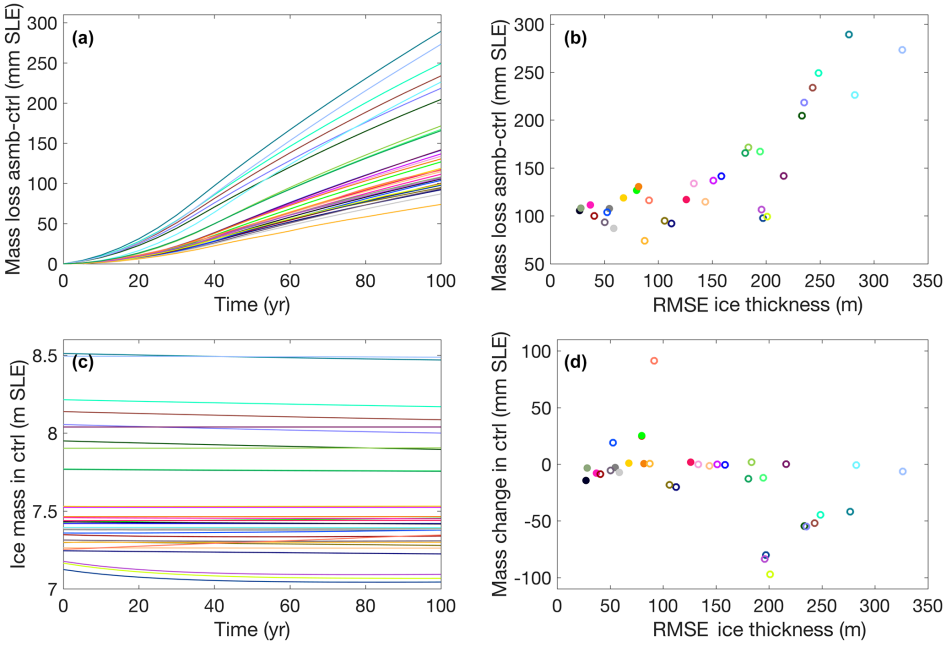

Figure 8. Ice mass evolution in ctrl **(a)** and ice mass loss from asmb–ctrl **(c)**. Mass change after 100 years in experiment ctrl **(b)** and from asmb–ctrl **(d)** related to error in initial ice thickness. Ice volume changes have been converted to sea-level equivalent (SLE) assuming an ocean area of 361.8×10^6 km^2 and the specific ice density from the individual ice sheet models. Filled symbols in **(b)** and **(d)** represent DAv models. Data in **(b)** and **(d)** are available in Supplement Table S1.

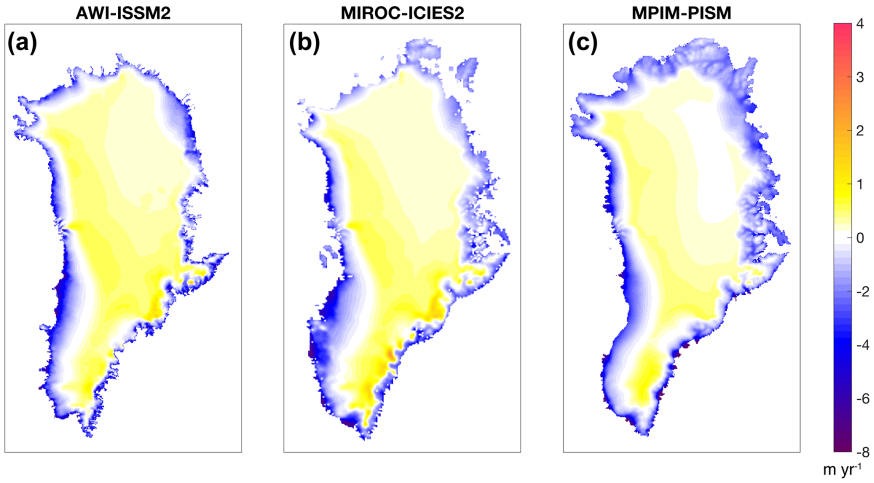

Figure 9. Typical surface mass balance after 100 years in experiment asmb for the three models in Fig. 3. Note the unequal scaling for positive and negative values.

periment are therefore complementary measures that should be considered together. While this is evident for any single model, we only find tentative confirmation amongst the DAv models in our ensemble (filled symbols in Fig. 8b), with increasing mass trend for decreasing ice thickness error.

The simulated sea-level contribution of the models, calculated from the difference in mass change between asmb and ctrl, shows a large spread of 75 to 290 mm SLE (Fig. 8c, d), indicative of the wide range of modelled ice sheet extent (and therefore ice thickness error). This relation arises because the prescribed SMB anomaly has been optimised for the observed geometry but has not been limited to the observed ice sheet extent. The typical SMB field at the end of experiment asmb (illustrated for three different models in Fig. 9) is strongly negative along the ice sheet margin, with an ablation zone that covers all of the ice sheet margin and extends several hundred kilometres inland in the southwest and northeast of Greenland. For models with (unrealistically) large initial (present-day) surface areas, the ablation zones are considerably larger (Fig. 9b, c), which implies dramatic mass loss. The too-large ice sheet area is not only related to the definition of the ice sheet with respect to outlying glaciers; more importantly, it is also due to modelled initial conditions further from the present day. Simply put, by design a larger ice sheet will be subject to larger rates of mass loss.

The spatial patterns of thickness changes in experiment ctrl (Figs. 10a, b, c and S5) clearly reflect some important differences and similarities between the models and the initialisation techniques used. DA models typically exhibit more noise (e.g. Fig. 10a) than SP models (e.g. Fig. 10b, c), which arises from inconsistencies between geometry and velocity for the former as discussed above. Models with identical model setup, but at different horizontal resolution, show similar patterns, and the same applies for different versions of one model (DMI-PISM), which differ only by the PDD parameters (Fig. S5). In all cases, thickness changes are the largest close to the margin and less pronounced in the interior of the ice sheet, a difference that becomes clearer with longer relaxation time. The patterns also confirm that positive and negative thickness changes at different locations often compensate for each other so that the total mass change in experiment ctrl (Fig. 8c and Table S1) is not a complete measure of the model drift. Because the thickness change in experiment ctrl is mostly due to unwanted model drift, we have calculated the mass evolution (Fig. 8c) and sea-level contribution (Fig. 8d) from ice thickness change differences between asmb and ctrl (Figs. 10d, e, f and S6). This is a common workaround to remove model drift and facilitate model comparison, but it also neglects the contribution of any prognostic imbalance and present-day ice sheet evolution in the resulting figures. In the centre of the ice sheet, the modelled thickness change (Fig. 10d, e, f) is dominated by the prescribed SMB anomaly and therefore similar between all models (Fig. S6), while marginal changes again show much larger differences.

In contrast to the large differences in modelled ice volume changes, which may largely be explained by differences in initial ice sheet extent, we find that models are similar in the dynamic response within the region of overlap, i.e. within most of the observed ice mask. For this analysis, we have calculated the difference between modelled ice thickness changes (asmb–ctrl) and the time-integrated SMB anomaly for each individual model (see Fig. 10g, h, and i for three examples and Fig. S7 for all models). This diagnostic, first shown and discussed by Huybrechts et al. (2002), represents ice thickness changes due to the flow of the ice in response to changes in SMB; in other words, the extra information gained by using ice dynamic models over projections of SMB changes alone.

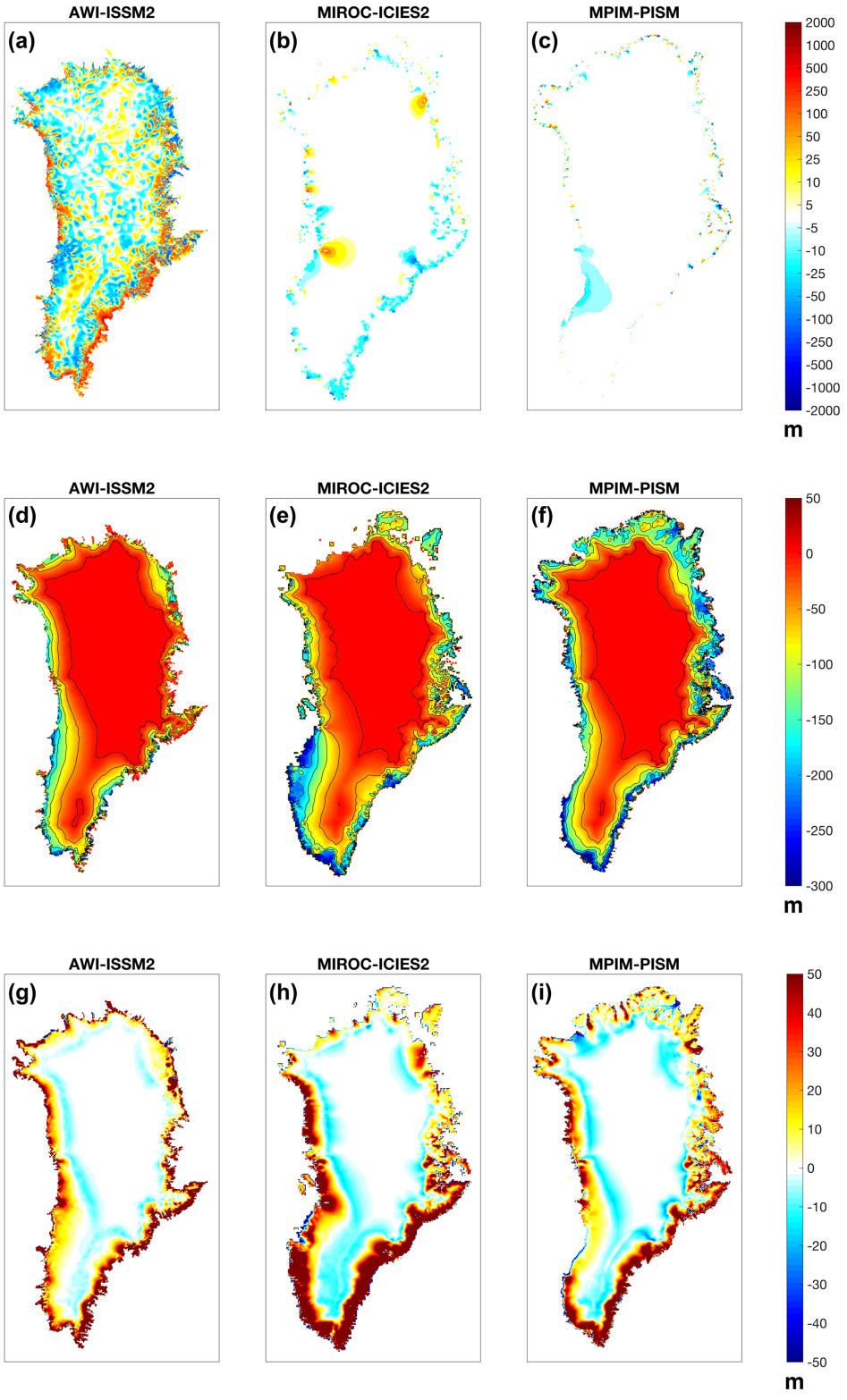

Figure 10. Ice thickness change in ctrl after 100 years **(a, b, c)**, difference of ice thickness change (asmb–ctrl) after 100 years **(d, e, f)**, and dynamic contribution **(g, h, i)** for the three models in Figs. 3 and 9. Note the non-linear contour intervals in the top row.

Dynamic thickening happens in regions of steep gradients in negative SMB anomalies around the margins of the ice sheet. Dynamic thinning occurs across the line separating positive and negative SMB anomalies, close to the equilibrium line. This pattern of dynamic response is reproduced by all models (see Fig. S7) and shows strong similarities for the region of overlap across the entire ensemble. In other words, the models largely agree in their representation of the ice dynamical response to the applied SMB anomaly forcing.

5 Discussion and conclusion

We have compared different initialisation techniques used in the ice sheet modelling community across a representative spectrum of approaches. While long-term processes and adjustment of internal variables (e.g. ice temperature and rheology) can be incorporated with SP methods, this occurs at the expense of a better match with observations of present-day ice sheet geometry and velocity and, hence, the initial dynamic state of the ice sheet. Conversely, the initial states produced by the DAv approach exhibit a much better match with observations, at the expense of including long-term processes. The DAs method and other approaches to incorporate DA elements in SP models and vice versa form an intermediate group. At present, none of the methods is capable of combining both aspects (good match with observations and long-term continuity) sufficiently well that it would render other methods obsolete for all applications.

DAv is the method of choice for short-term projections with anomaly forcing and as far as long-term dynamical interactions (e.g. arising from interaction with the basal conditions, from the bedrock, or from thermo-mechanical coupling) can be neglected. For long-term projections of ice sheet behaviour, where these interactions become important, SP and DAs methods are needed. The range of timescales where this is the case is not well defined and may lie anywhere between several decades and several centuries. For the stand-alone ice sheet projections planned for CMIP6 within ISMIP6 (100- to 200-year timescale), a combination of SP and DA methods may be required to simulate the response of the Greenland ice sheet to future climate change. The challenge remains how to initialise models to closely match the observed dynamical state and at the same time minimise unrealistic transients and incorporate the long-term evolution of thermodynamics and bedrock changes. A promising approach is additionally optimising the basal topography within observational errors as part of the data assimilation procedure (Perego et al., 2014; Mosbeux et al., 2016). Other approaches, based on assimilation of time series of observed surface velocity (Goldberg and Heimbach, 2013) or surface elevations (Larour et al., 2014) exist for smaller scales but should be further explored to eventually be applied over the entire ice sheet. A so-far-underexplored possibility is to use existing information from radar layers (MacGregor et al., 2015) as additional constraints in initialisation methods.

The present "come-as-you-are" approach is well suited to produce an overview of initialisation techniques in the community and to compare individual models against observations. However, we have encountered difficulties in comparing models because of the wide variety of approaches. Differences in the initial ice sheet extent have rendered the locally identical SMB anomaly forcing to be different on the global scale. We have found that estimating mass changes consistently across all models becomes a non-trivial undertaking, considering differences in ice sheet masks, projection errors, and differences in model ice density. Additional problems arise from the use of different native grids (unstructured and structured) with potential artefacts introduced by interpolation that we have not been able to quantify.

The mismatch between observed and modelled ice sheet extent also needs an urgent solution in view of constructing an ensemble of sea-level change projections based on CMIP6 climate model data. The large ensemble spread in sea-level contribution in the asmb experiment is mostly due to the "extra" ice in the initial ice sheet geometry. At this stage, it is not clear how to minimise the contribution to sea-level change due to this bias introduced solely by the experimental setup. Letting each model estimate its own SMB anomaly relative to the individual ice sheet geometry would likely reduce this problem, but it would complicate any further comparison by removing the constraint of locally identical SMB for all models.

Compared with earlier ice sheet model intercomparison exercises that have initialised ice sheet models for future projections (Bindschadler et al., 2013; Nowicki et al., 2013b), we find considerably less drift in the control experiments (for models that also participated in previous intercomparisons). We attribute this improvement to more attention of modellers on ice sheet initialisation and to an improved understanding of what is needed to achieve that goal, including the development of improved bedrock topography data sets (Morlighem et al., 2014). If this trend continues and initialisation methods get further developed, it is reasonable to expect that the uncertainty in simulated ice sheet model evolution due to initialisation can be reduced for upcoming projections of the future.

The comparison shows that, despite all the differences, the ice sheet models that took part in this intercomparison agree well in their dynamic response to the SMB forcing for the region of overlap. This is an encouraging sign, given the large diversity of approaches. However, while this good agreement means that all models are able to accurately simulate changes in driving stress, other dynamic forcings (e.g. changes at the marine-terminating glaciers) were not included in the present set of experiments and may lead to a wider variety of responses. To achieve progress in this direction, we need a more complete understanding of the forcings and mechanisms that drive observed ice sheet changes. Aside from

SMB, the important questions of how much surface meltwater is reaching the bed; how the basal drainage system evolves; and, most importantly, how the marine-terminating glaciers interact with the ocean in fjord systems are under active research.

The current "ensemble-of-opportunity" approach, just as for general circulation models (GCMs), makes interpretation challenging: in other words, it is difficult to assess which choices in method and which uncertain model inputs have most influence on the results. Ideally, we would have liked to draw firmer conclusions about the influence of modelling choices on the quality of the initialisation and the uncertainty in modelled sea-level contribution. At the present stage, however, the sample size for a given modelling choice is often not sufficient and, more importantly, different model characteristics are not independent from each other. Similar difficulties have been discussed for the CMIP multi-model ensemble and may have led to the IPCC to resort to (slightly arbitrary) expert judgments for some interpretations. Improving the uncertainty analysis and enabling a more rigorous intercomparison and evaluation would require an experimental design that is more controlled and prescriptive. Ice sheet models are well placed to be used in such a design, being far less computationally expensive than, for example, GCMs and having far fewer inputs to choose and outputs to evaluate. The effects of changing model structure (such as physics laws and approximations, and resolution) on initialisations and projections is also far easier to evaluate. We therefore envision a second stage of the initMIP-Greenland experiments that performs multiple specific perturbations of the initial states of several models that can be interpreted in a statistically more meaningful way.

Data availability. The model output from the simulations described in this paper will be made publicly available with a digital object identifier (DOI) https://doi.org/10.5281/zenodo.1173088. In order to document CMIP6's scientific impact and enable ongoing support of CMIP, users are obligated to acknowledge CMIP6, ISMIP6 and the participating modelling groups. The forcing data sets are equally made publicly available via https://doi.org/10.5281/zenodo.1173088.

Appendix A: SMB anomaly forcing

For the idealised forward experiment that serves to evaluate the initialisation, we have used a parameterisation of SMB anomalies (dSMB) as a function of surface elevation and latitude based on the following goals:

- to capture the first-order pattern of the SMB changes that can be expected from the climate models that will be used in ISMIP6 projections;
- to provide an idealised forcing, independent of one particular model or modelling choice;
- to avoid masking problems by generating a forcing applicable to the whole model domain.

The parameterisation has the form dSMB $= f(\mathrm{sur}, \mathrm{lat})$:

$$\mathrm{dSMB} = \min[p_3 \cdot (h - p_2) + p_4 \cdot (\phi - \phi_0), p_1],$$

where dSMB is the SMB anomaly, h is the surface elevation, ϕ is the latitude, and ϕ_0 is the reference latitude in degrees. The parameters are the constant SMB anomaly in the accumulation area (p_1), the surface elevation of zero SMB anomaly (p_2), the gradient of SMB anomaly with elevation change (p_3), and the SMB anomaly change per degree latitude (p_4).

The target dSMB is calculated from differences in SMB between the periods 2080–99 AD and 1980–99 AD. We have fitted the parameters independently to output of three models of different complexity (Table A1), one RCM (Fettweis et al., 2017), one GCM with elevation classes (Vizcaino et al., 2015), and one positive-degree-day model in combination with output from an Earth system model of intermediate complexity (EMIC-PDD; Goelzer et al., 2012).

The sensitivity of dSMB to elevation changes is around a factor of 2 lower in the GCM than in the RCM and is the highest in EMIC-PDD as can be seen by comparing p_3 in Table A1. We have used the parameter set of medium sensitivity (RCM) for the experiments.

Results for the RCM are shown in Fig. A1 with the dSMB from the model (a) and from the parameterisation (b) in comparison. While the parameterisation allows for calculating dSMB everywhere on the grid, results are masked to the same extent as the modelled data, to facilitate comparison. These results show that the first-order pattern is well captured by the parameterisation. The parameterisation works equally well for the two other climate models when proper masking is applied to limit the calculation to ice-covered regions (not shown).

For the final ISMIP6 forcing data, the parameterisation was applied to the observed geometry (Bamber et al., 2013) smoothed by a two-dimensional averaging filter (21 × 21 points). This step serves to produce a smooth forcing field for the range of expected model resolutions. The resulting

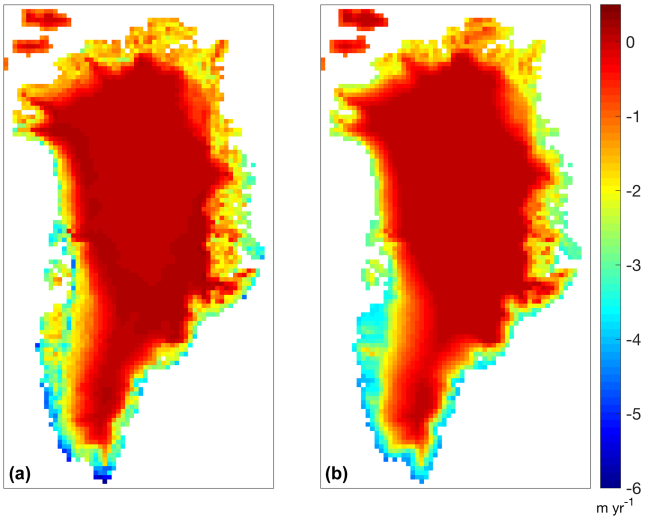

Figure A1. SMB anomaly from a model **(a)** and reproduced by the parameterisation **(b)**.

dSMB at 1 km resolution was used to generate the forcing for other grids and resolutions by conservative interpolation.

For experiment asmb, the amplitude of the SMB anomaly was implemented as a time-dependent function, which increases stepwise every full year to 100 % at year 40. The amplitude is then held constant ($t > 40$ years) for prolongation of the experiment until year 100. The forcing is therefore independent of the time step in the individual models:

$$\mathrm{SMB}(t) = \mathrm{SMB}_{\mathrm{init}} + \mathrm{dSMB} \cdot (\mathrm{floor}(t)/40); \quad 0 \le t \le 40$$
$$\mathrm{SMB}(t) = \mathrm{SMB}_{\mathrm{init}} + \mathrm{dSMB} \cdot 1.0; \quad t \ge 40,$$

where $\mathrm{SMB}_{\mathrm{init}}$ is the SMB used for the initialisation in each individual model and dSMB is the provided SMB anomaly, which is identical for all models. The units of the dSMB in the provided data files are metre ice equivalent per year with an assumed density of $910\,\mathrm{kg\,m^{-3}}$ and $31\,556\,926\,\mathrm{s\,yr^{-1}}$. Note that, for models assuming a different ice density, the input data have to be converted accordingly.

Appendix B: Detailed model description

The models and initialisation methods of the individual models are documented in this section.

B1 ARC-PISM

A similar approach to that used for previous Antarctic simulations is followed (e.g. Golledge et al., 2014, 2015), but the length of the runs is modified on the basis that GrIS achieves thermal equilibrium faster than, for example, the East Antarctic Ice Sheet. Based on raw input data (Bamber et al., 2001) a "shallow-ice-only" run of 5 years is performed to reduce any spurious steep surface gradients in the data.

Table A1. Parameters with the best fit to the modelled data for SMB models of different complexity.

Parameter	p_1 ($\mathrm{m\,yr^{-1}}$)	p_2 (m)	p_3 ($\mathrm{m\,yr^{-1}\,m^{-1}}$)	p_4 ($\mathrm{m\,yr^{-1}\,deg^{-1}}$)
RCM	0.0720	2248.4	0.0016	0.1011
GCM	0.0549	2438.1	0.0007	0.0568
EMIC-PDD	0.0292	1642.1	0.0023	0.0462

From the output of this run, a 50 kyr fixed-geometry run is performed, in which the ice sheet is allowed to come into thermal equilibrium with the imposed (present-day) climate. The output from this run is then used for a 15 000-year spin-up simulation, in which full model physics are employed; i.e. all model boundaries are allowed to evolve. To minimise drift in this spin-up run an initial exploration of parameter space is undertaken to find an optimal combination of values. Parameter tuning is focused on six key controls: enhancement factors for the shallow-ice approximation (SIA) and shallow-shelf approximation (SSA), maximum and minimum till friction angles, pseudo-plastic exponent "q", and the fraction of overburden pressure supported by the till. These parameters have been found to exert the primary controls on location and magnitude of sliding and ice flow by deformation, and in doing so most effectively control simulated ice sheet geometry and volume. To identify an optimal configuration, an initial ensemble of paired parameter simulations is performed, in which the variance between each pair is assessed and all other variables are held constant. Simulations are run at 5 km resolution for 500 years under unforced climatic conditions (i.e. present day) but with freely evolving boundaries. Each run is assessed for degree of drift from initialisation. Subsetting from these experiments, a further ensemble of 64 experiments is run, combining all combinations of two possible values for each of the six parameters. The "optimal" configuration is chosen based on (1) the lowest deviation from present-day sea-level-equivalent ice volume and (2) the smallest domain-averaged thickness mismatch at the end of the run compared to initialisation. For the latter metric, the standard deviation of the mismatch was assessed, but differences between runs are minimal. These short runs identify the relative control exerted by each parameter over 500 years. To achieve a much longer spin-up that deviates least from the starting conditions, a further seven experiments are undertaken until the optimum parameter configuration is found. The final state of the spin-up run is then used as the starting point for the prognostic (ctrl and asmb) experiments.

B2 AWI-ISSM

The thermo-mechanical coupled Ice Sheet System Model (ISSM; Larour et al., 2012) is used to create an initial condition. For the initialisation, a hybrid procedure that combines assimilation and a temperature spin-up over longer periods is set up. The present-day ice sheet geometry (Morlighem et al., 2014) is used, and the observed horizontal surface velocities (Rignot and Mouginot, 2012) are assimilated to infer the basal friction coefficient. After an initial relaxation of the ice sheet geometry for 50 years to avoid spurious noise (with no sliding and a constant temperature field), the temperature spin-up is performed on a fixed topography with two different climatic forcings: present-day climate (AWI-ISSM1) and palaeoclimatic conditions (AWI-ISSM2). During the inversion, the ice viscosity is kept constant using the enthalpy field from the end of the temperature spin-up. As the higher-order approximation to the Stokes flow is employed, grid refinements are made during the whole initialisation procedure (grid sequence 1: hmin = 15 km, hmax = 50 km; grid sequence 2: hmin = 5 km, hmax = 50 km; grid sequence 3: hmin = 2.5 km, hmax = 35 km. In the vertical, 17 layers refined to the base are used. AWI-ISSM1 is run for 20, 40, and 5 kyr in each grid sequence, while AWI-ISSM2 is run for 125, 125, and 25 kyr). Geothermal flux, present-day surface temperature, and palaeo-surface-temperature anomaly are taken from the SeaRISE website (http://websrv.cs.umt.edu/isis/index.php/Present_Day_Greenland). Surface mass balance is an annual mean for the period 1979–2014 from the downscaled RACMO2.3 model (Noël et al., 2016).

B3 BGC-BISICLES

The initial state is found using data assimilation of velocity followed by relaxation of the surface elevation subject to a constant-in-time SMB (Lee et al., 2015). Merged surface ice velocity from Rignot and Mouginot (2012) is used to infer a 2-D basal traction coefficient and a 2-D stiffening factor multiplying the effective viscosity by solving an inverse problem with fixed ice sheet geometry from Morlighem et al. (2014). The ice surface is evolved by forcing the model using the 2-D parameters with a 1997–2006 mean SMB from HIRHAM5 (Lucas-Picher et al., 2012), subject to fixed calving front boundary conditions. The surface is relaxed in this way for 120 years, which is sufficient for the absolute value of the instantaneous rate of change of the ice thickness to fall below 0.5 m $\mathrm{a^{-1}}$ in 99 % of the total area of GrIS. This initialisation uses a 3-D steady-state temperature field generated by a high-order thermomechanical model by Price et al. (2011). For the ctrl and asmb experiments the fixed calving front is replaced by a calving model (Taylor, 2016), where ice calves if water-filled, surface crevasses reach a depth equal to the height of the ice above sea level. A basal melt rate varying

between 0 and 4 times the ice thickness is also applied in regions where ice is close to fracture.

B4 DMI-PISM

A spin-up over one full glacial cycle (125 kyr BP to present) is performed with the following guidelines: a freely evolving run that inherits the climate memory of the last glacial–interglacial cycle and shall represent the currently observed ice sheet state for the contemporary "year of assignment". Since we at DMI focus on coupled climate model–ice sheet model simulations, we value a free run that is consistent with the applied forcing higher than a perfect representation of the current observed Greenlandic ice sheet state, such as ice sheet geometry. We have found that this procedure is necessary to avoid strong unnatural drifts in the ice sheet model component after the full coupling between the climate model and the ice sheet model is established (Svendsen et al., 2015). The spin-up first goes through one complete glacial–interglacial cycle using as a basis the ERA-Interim reanalysis of the period 1979–2012 to determine the SMB via PDDs. The scaling of the data sets is determined based on the Greenland temperature index in the SeaRISE Greenland data set (based on ice core data; source SeaRISE reference data set: Greenland_SeaRISE_dev1.2.nc). Temporal evolution of the sea level is also taken from the same SeaRISE Greenland data set. The ensemble of runs (PISM1, PISM2, PISM3, PISM4, PISM5) differs in the forcing applied to the GrIS. In all cases the forcing source is based on the ERA-Interim reanalysis covering the period 1979–2012. The only differences are the applied PDD factors for the determination of the SMB via PDDs. The following enumeration lists the applied different PDD factors: PISM0: PDD_snow $= 0.012\,\mathrm{m\,C^{-1}\,day^{-2}}$, PDD_ice $= 0.018\,\mathrm{m\,C^{-1}\,day^{-2}}$; PISM1: PDD_snow $= 0.010\,\mathrm{m\,C^{-1}\,day^{-2}}$, PDD_ice $= 0.016\,\mathrm{m\,C^{-1}\,day^{-2}}$; PISM2: PDD_snow $= 0.009\,\mathrm{m\,C^{-1}\,day^{-2}}$, PDD_ice $= 0.014\,\mathrm{m\,C^{-1}\,day^{-2}}$; PISM3: PDD_snow $= 0.008\,\mathrm{m\,C^{-1}\,day^{-2}}$, PDD_ice $= 0.012\,\mathrm{m\,C^{-1}\,day^{-2}}$; PISM4 PDD_snow $= 0.004\,\mathrm{m\,C^{-1}\,day^{-2}}$, PDD_ice $= 0.008\,\mathrm{m\,C^{-1}\,day^{-2}}$.

B5 IGE-ELMER

The model is initialised using an inverse control method as in Gillet-Chaulet et al. (2012). For the momentum equations, we solve the shelfy-stream approximation. The vertically averaged viscosity is constant in all simulations and is initialised using the temperature field coming from a palaeo-spin-up (125 kyr) of the SICOPOLIS model. The limit of the model domain is fixed and corresponds to the boundary with the ocean: calving front positions are fixed, and the calving rate is computed as the opposite of the ice flux through the boundary; land-terminated parts can freely retreat or advance up to the domain limit. The ice sheet topography is initialised using the IceBridge BedMachine Greenland V2 data set (Morlighem et al., 2014, 2015), where missing values for the bathymetry around Greenland have been filled using data from Bamber et al. (2013). We use a linear basal friction law. The basal friction coefficient is constant in all transient simulations and is initialised with the control method so that the mismatch between observed and modelled velocities is minimum. As observations, we use a composite from the NASA Making Earth System Data Records for Use in Research Environments (MEaSUREs) Greenland Ice Sheet Velocity Map (V1) (Joughin et al., 2010a, b). The ice sheet model is then relaxed for 20 years using a 1989–2008 mean SMB from the regional climate model MAR (Fettweis et al., 2017) forced with ERA-Interim. The only difference between IGE-ELMER1 and IGE-ELMER2 is the mesh resolution as given in Table 3.

B6 ILTS-SICOPOLIS

The model is SICOPOLIS version 3.3-dev in SIA mode and with the melting-cold-temperature transition surface enthalpy method for ice thermodynamics by Greve and Blatter (2016). The present-day surface temperature parameterisation is by Fausto et al. (2009), the present-day precipitation is by Ettema et al. (2009), and the geothermal heat flux is by Greve and Herzfeld (2013) (slightly modified version of the heat flux map by Greve, 2005). A spin-up over the last glacial–interglacial period (125 000 years) is carried out. Except for initial and final 100-year phases with freely evolving surface and bedrock topography, the topography is kept fixed during the spin-up, whereas the temperature evolves freely. This is essentially the method that was used for the SeaRISE experiments (documented in detail by Greve and Herzfeld, 2013). The time-dependent forcing for the spin-up is the GRIP δ^{18}O record (Dansgaard et al., 1993; Johnsen et al., 1997) converted to a purely time-dependent surface temperature anomaly ΔT by the conversion factor $2.4\,^{\circ}\mathrm{C}\,‰^{-1}$ (Huybrechts, 2002).

B7 ILTSPIK-SICOPOLIS

The model version, thermodynamics solver, and present-day surface temperature parameterisation are the same as listed in Sect. B6. The present-day precipitation is by Robinson et al. (2010), and the geothermal heat flux is produced by Purucker (https://core2.gsfc.nasa.gov/research/purucker/heatflux_updates.html) following the technique described in Fox Maule et al. (2005). The bedrock topography is from Herzfeld et al., (2014). The ice discharge parameterisation by Calov et al. (2015), Eq. (3) therein with the discharge parameter $c = 370\,\mathrm{m^3\,s^{-1}}$, is applied. A spin-up over the last glacial–interglacial period (135 000 years) with free evolution of all fields (including the ice sheet topography) is carried out. The time-dependent forcing for the spin-up is the GRIP δ^{18}O record (Dansgaard et al., 1993; Johnsen et al.,

1997) on the GICC05 timescale (Svensson et al., 2008), converted to a purely time-dependent surface temperature anomaly ΔT by the conversion factor $2.4\,^{\circ}\mathrm{C}\,‰^{-1}$, and further a 7.3 % gain of the precipitation rate for every 1 °C increase of ΔT (Huybrechts, 2002).

B8 IMAU-IMAUICE

The model (de Boer et al., 2014) is initialised to a thermodynamically coupled steady state with constant present-day boundary conditions for 200 kyr using the average 1960–1990 surface temperature and SMB from RACMO2.3 (van Angelen et al., 2014), extended to outside of the observed ice sheet mask using the SMB gradient method (Helsen et al., 2012). Bedrock data are from Bamber et al. (2013), and geothermal heat flux data are from Shapiro and Ritzwoller (2004). The model is run in SIA mode with ice sheet margins evolving freely within the observed coast mask, outside of which ice thickness is set to zero.

B9 JPL-ISSM

The ice sheet configuration is set up using data assimilation of present-day conditions and historical spin-up similar to the study of Schlegel et al. (2013). SSA is used over the entire domain with a resolution varying between 1 km in the fast-flowing areas and along the coast and 15 km in the interior. Grounding line migration is based on hydrostatic equilibrium and a sub-element scheme (Seroussi et al., 2014). Observed surface velocities (Rignot and Mouginot, 2012) are first used to infer unknown basal friction at the base of the ice sheet (Morlighem et al., 2010). Ice temperature is modelled assuming the ice sheet to be in a steady-state thermal equilibrium (Seroussi et al., 2013). A spin-up of 50 000 years is then done to relax the ice sheet model (Larour et al., 2012) and reduce the initial unphysical transient behaviour due to errors and biases in the data sets (Schlegel et al., 2016) using mean surface mass balance from 1979 to 1988 (Box, 2013). A historical spin-up is then done from 1840 to 2012 using reconstructions of surface mass balance for this period (Box, 2013). Bedrock topography is interpolated from the BedMachine data set (Morlighem et al., 2014), which combines a mass conservation algorithm for the fast-flowing ice streams and kriging in the interior of the ice sheet. Initial ice thickness is from the Greenland Ice Mapping Project (GIMP) data set (Howat et al., 2014). Geothermal flux is from Shapiro and Ritzwoller (2004); air temperature is from RACMO2 (van Angelen et al., 2014). SMB from a mass balance reconstruction (Box, 2013) averaged over the 2000–2012 period is used in the ctrl experiment.

B10 LANL-CISM

The ice sheet was initialised with present-day geometry and an idealised temperature profile, and then spun up for 20 000 years using pre-1990 climatological surface mass balance and surface air temperature from RACMO2. No glacial data were used. The model was spun up for 20 000 years to equilibrate the temperature and geometry with the forcing. The model was initialised (prior to spin-up) with present-day topography and thickness based on the mass-conserving bed method of Morlighem et al. (2011). The SMB over the ice sheet was a 1961–1990 climatology from RACMO2. In grid cells where RACMO2 did not provide an SMB, the SMB was set arbitrarily to $-2\,\mathrm{m\,yr^{-1}}$. Surface air temperatures were also from a 20th-century RACMO2 climatology (Ettema et al., 2009). The geothermal flux was set spatially uniform to $0.05\,\mathrm{W\,m^{-2}}$.

B11 LSCE-GRISLI

The GRISLI spin-up procedure is based on an iterative data assimilation method to infer the basal drag from the observed surface velocities. The first step consists of a 30 kyr equilibrium simulation of the internal temperature with prescribed ice sheet topography (Bamber et al., 2013), 1979–2005 averaged near-surface air temperature (Fettweis et al., 2017), geothermal heat flux (Fox Maule et al., 2005), surface velocities (Joughin at al., 2013), and spatially variating basal drag coefficient from a previous GRISLI experiment (Edwards et al., 2014b). From the resulting internal fields, the 1979–2005 mean SMB and near-surface air temperature (Fettweis et al., 2017) are used to run a succession of eight 220 yr simulations. During the first 20 years, the basal drag coefficient is corrected to limit the deviation from prescribed velocities, and then the basal drag is kept constant for 200 years of surface relaxation. At each iteration, we update the basal drag coefficient with the value computed at the previous iteration. The prescribed velocities are the observed velocities corrected for thickness differences at the end of the 220 years in order to keep the ice flux in GRISLI identical to the observed one. Then, a second temperature equilibrium is run for consistency between the temperature field and the inferred basal drag coefficient. From this, an additional 220 yr simulation is run to optimise the final basal drag coefficient. This basal drag coefficient and associated final ice sheet conditions are used as initial conditions for all the initMIP GRISLI experiments.

B12 MIROC-ICIES1

The simulation set-up of MIROC-IcIES1 is described in Appendix A of Saito et al. (2016), as the experiment E″s:e1:vm. The surface mass balance field to force the ice sheet model follows the present-day field provided by SeaRISE, without any correction except for the horizontal resolution. This mass balance is computed using a PDD method, and the parameters are described at http://websrv.cs.umt.edu/isis/index.php/Future_Climate_Data. The field of basal sliding coefficients are relaxed such that the simulated ice sheet topography under the present-day surface mass balance field mostly

matches the observed geometry, using the method by Pollard and DeConto (2012b). Using the deduced basal sliding coefficients field, a steady-state spin-up under present-day climate conditions with the fixed geometry is performed again while the temperature evolves freely.

B13 MIROC-ICIES2

The simulation set-up of MIROC-IcIES2 is described in Saito et al. (2016), as the experiment B′:v2. A free spin-up over 125 000 years is performed following the SeaRISE configuration: the background temperature history based on the oxygen isotope record of the GRIP ice core is used as an anomaly to the present-day field. During the spin-up, the ice sheet margin is allowed to freely advance and retreat. The present-day surface temperature follows the parameterisation presented in Fausto et al. (2009). The present-day mean annual precipitation follows Ettema et al. (2009). The surface mass balance is computed using these fields and a PDD method whose coefficients follow those in Huybrechts and de Wolde (1999). The basal sliding velocity is computed using the Weertman sliding law, with an allowance for sub-melt sliding following Hindmarsh and Le Meur (2001). The parameters are kept constant and follow those in Huybrechts and de Wolde (1999) except that the coefficient is doubled to obtain a better match with the present-day topography.

B14 MPIM-PISM

A spin-up over one full glacial cycle (135 kyr BP to present) is performed, where model parameters are changed at 20 kyr BP. It is faster to start from a pre-spun up state at 20 kyr BP than to re-run the full glacial cycle for each parameter change. The spin-up first goes through one complete glacial cycle using a linear combination of MPI-ESM output. The scaling of the two data sets is determined based on the Greenland temperature index in the SeaRISE Greenland data set (based on GRIP data). Sea-level changes are also taken from the SeaRISE Greenland data set.

B15 UAF-PISM

A spin-up over a glacial cycle is combined with a short relaxation run. To define the energy state, a "standard" glacial cycle run is performed where the surface can evolve freely, similar to Aschwanden et al. (2013) and Aschwanden et al. (2016). The spin-up starts at 125 kyr BP with the present-day topography from Howat et al. (2014) using a horizontal grid resolution of 9 km. The grid is refined to 6, 4.5, and 3 km at 25, 20, and 15 kyr BP, respectively. We use a positive-degree-day scheme to compute the climatic mass balance from surface temperature (Fausto et al., 2009) and model-constrained precipitation (Ettema et al., 2009). The degree-day factors are the same as in Huybrechts (1999). Second, we account for palaeoclimatic variations by applying a scalar anomaly term derived from the GRIP ice core oxygen isotope record (Dansgaard et al., 1993) to the temperature field (Huybrechts, 2002). Then we adjust mean annual precipitation in proportion to the mean annual air temperature change (Huybrechts, 2002). Finally, sea-level forcing, which determines the land area available for glaciation, is derived from the SPECMAP marine δ^{18}O record (Imbrie et al., 1992). At the end of the spin-up, the computed surface elevation differs from the observed surface elevation. From here we perform two sets of 60-year relaxation simulations using the RACMO 1960–1990 averaged climatic mass balance. In one set (UAF-PISM4–6), we regrid the spun-up state from the 3 km simulation to 1.5 km (UAF-PISM4), 3 km (UAF-PISM5) and 4.5 km (UAF-PISM6) and run a relaxation where the ice sheet is free to evolve. At the end of this relatively short relaxation, the computed surface elevation continues to differ substantially from present-day observation, and the model states exhibit a large artificial drift. To reduce the mismatch between observed and simulated surface elevations, we perform a second set, UAF-PISM1–3. Here we regrid the energy state in the ice and in the bedrock from the spun-up state from the 3 km simulation to 1.5 km (UAF-PISM1), 3 km (UAF-PISM2), and 4.5 km (UAF-PISM3) and combine those fields with the present-day topography from Howat et al. (2014) to again run a relaxation where the ice sheet is free to evolve.

B16 UCIJPL-ISSM

The ice sheet configuration is set up using data assimilation of present-day conditions (Morlighem et al., 2010). A relaxation of 50 years is then performed to reduce the initial unphysical transient behaviour due to errors and biases in the data sets (Seroussi et al., 2011), using mean surface mass balance from 1961 to 1990 (van Angelen et al., 2014). A higher-order model (HO) is used for the entire domain, with 14 vertical layers and a horizontal resolution varying between 0.5 km along the coast and 30 km inland. We perform the inversion of basal friction assuming that the ice is in thermomechanical steady state. The ice temperature is updated as the basal friction changes, and the ice viscosity is changed accordingly. At the end of the inversion, basal friction, ice temperature, and stresses are all consistent. After the data assimilation, the model is relaxed for 50 years using the mean surface mass balance of 1961–1990 from RACMO (van Angelen et al., 2014), while keeping the temperature constant. Bed topography is interpolated from the BedMachine Greenland v3 data set (Morlighem et al., 2017), which combines a mass conservation algorithm for the fast-flowing ice streams and kriging in the interior of the ice sheet. Initial ice surface topography is from the GIMP data set (Howat et al., 2014). For the thermal model, surface temperatures from Fausto et al. (2009) and geothermal heat flux from Shapiro and Ritzwoller (2004) are used. Mean surface mass balance of 1961–1990 from RACMO (van Angelen et al., 2014) is used in the ctrl experiment.

B17 ULB-FETISH

Model initialisation is based on the method by Pollard and DeConto (2012b) by optimising basal sliding coefficients for the grounded ice sheet in an iterative way through minimising the misfit between observed and modelled surface topography. A regularisation term is introduced to smooth high-frequency noise in the basal sliding coefficients (Pattyn, 2017). Initial ice sheet surface and bedrock elevation are taken from Bamber et al. (2013), and geothermal heat flux stems from Fox Maule et al. (2009). The initialisation runs over a period of 50 000 years forced by a constant surface mass balance (Fettweis et al., 2007) and surface temperature (Fausto et al., 2009). During this time, the marine boundaries are kept fixed in space. For the control and forcing runs, the grounded ice margin and grounding line are allowed to move freely, starting from the initialised state. Two model setups were considered: FETISH1 is according to SIA; FETISH2 is a hybrid model (superimposed SSA-SIA) with a flux condition at the grounding line according to Schoof (2007) and Pollard and DeConto (2012a).

B18 VUB-GISM

The model is initialised with a glacial spin-up over the last two glacial cycles and recent climate forcing data up to the year 2005 (Fürst et al., 2015). For the spin-up, a synthesised temperature record is used based on ice core data from Dome C, NGRIP, GRIP, and GISP2 (Barker et al., 2011; Andersen et al., 2004; Dansgaard et al., 1993; Kobashi et al., 2011), and precipitation is scaled by 5 % per degree Celsius. For the period 1958 to 2005, the atmospheric forcing comes from a combination of European Centre for Medium-Range Weather Forecasts (ECMWF) ERA-Interim meteorological reanalysis and ECMWF operational analysis data. Use is made of monthly temperature anomalies and yearly precipitation ratios. The ocean forcing from 1958 to 2005 derives from a CMIP5 model providing temperature anomalies at mid-depth (300–800 m) in five surrounding ocean basins with respect to the 1960–1990 period. After the year 2005, atmospheric and oceanic forcings are reset to their 1960–1990 averages in the unforced state. Bedrock elevation and coast mask are based on Bamber et al. (2013); the pattern of surface accumulation for the period 1950–2000 is based on Bales et al. (2009). The higher-order model (GISM1) is initialised with an SIA model (GISM2) to 3 kyr BP. Switching at 3 kyr BP appeared to be sufficiently early to resolve the main effects of including horizontal stress gradients by the present day.

Appendix C: Data request

The requested variables (Table C1) serve to evaluate and compare the different models and initialisation techniques.

All 2-D data were requested on a regular grid with the following description: polar stereographic projection with standard parallel at 71° N and a central meridian of 39° W (321° E) on datum WGS84. The lower left corner is at (−800 000 m, −3 400 000 m), and the upper right at (700 000 m, −600 000 m). This is the same grid (Bamber et al., 2001) as used to provide the SMB anomaly forcing. The output was submitted on a resolution adapted to the resolution of the model and was 5 or 10 km. The data were conservatively interpolated to 5 km resolution for diagnostic processing.

If interpolation was required in order to transform the SMB forcing (1 km, same as Bamber et al., 2013) to the native model grid, and transform model output to the initMIP output grid (20, 10, 5, 1 km; Bamber et al., 2001), it was requested that conservative interpolation be used. The motivation for using a common method for all models is to minimise model-to-model differences due to the choice of interpolation methods. In most cases this has been followed by the modellers.

We distinguish between state variables (e.g. ice thickness, temperatures, and velocities) and flux variables (e.g. SMB). State variables were requested as snapshot information at the end of 1-year (scalars) and 5-year periods (2-D), while flux variables were averaged over the respective periods. For calculation of scalar diagnostics (e.g. total ice mass or ice-covered area), it is necessary to correct for the area distortions implicit for a given projection (e.g. Snyder, 1987). Some of the variables may not be applicable for each model, in which case they were omitted.

Please note that, in order to facilitate comparison with observational data sets and for consistency with future ISMIP6 activities, all model output data from initMIP-Greenland published to public archives have been conservatively interpolated to a new diagnostic grid. The grid uses EPSG:3413, a polar stereographic projection with standard parallel at 70° N and a central meridian of 45° W on datum WGS84.

Table C1. Data request for participation in initMIP-Greenland. Type: FL – flux variable; ST – state variable; CST – constant.

Variable name	Units	Type	Standard name (CF)
Ice sheet altitude	m	ST	surface_altitude
Ice sheet thickness	m	ST	land_ice_thickness
Bedrock altitude	m	ST	bedrock_altitude
Bedrock geothermal heat flux	$W\,m^{-2}$	CST	upward_geothermal_heat_flux_at_ground_level_in_land_ice
Surface mass balance flux	$kg\,m^{-2}\,s^{-1}$	FL	land_ice_surface_specific_mass_balance_flux
Basal mass balance flux	$kg\,m^{-2}\,s^{-1}$	FL	land_ice_basal_specific_mass_balance_flux
Land ice calving flux	$kg\,m^{-2}\,s^{-1}$	FL	land_ice_specific_mass_flux_due_to_calving
Ice thickness imbalance	$m\,s^{-1}$	FL	tendency_of_land_ice_thickness
X component of land ice surface velocity	$m\,s^{-1}$	ST	land_ice_surface_x_velocity
Y component of land ice surface velocity	$m\,s^{-1}$	ST	land_ice_surface_y_velocity
Z component of land ice surface velocity	$m\,s^{-1}$	ST	land_ice_surface_upward_velocity
X component of land ice basal velocity	$m\,s^{-1}$	ST	land_ice_basal_x_velocity
Y component of land ice basal velocity	$m\,s^{-1}$	ST	land_ice_basal_y_velocity
Z component of land ice basal velocity	$m\,s^{-1}$	ST	land_ice_basal_upward_velocity
X component of land ice vertical mean velocity	$m\,s^{-1}$	ST	land_ice_vertical_mean_x_velocity
Y component of land ice vertical mean velocity	$m\,s^{-1}$	ST	land_ice_vertical_mean_y_velocity
Surface temperature of ice sheet	K	ST	temperature_at_top_of_ice_sheet_model
Basal temperature of ice sheet	K	ST	temperature_at_base_of_ice_sheet_model
Basal drag	Pa	ST	land_ice_basal_drag
Land ice area fraction	1	ST	land_ice_area_fraction
Grounded ice area fraction	1	ST	grounded_ice_sheet_area_fraction
Floating ice shelf area fraction	1	ST	floating_ice_shelf_area_fraction
Ice mass	kg	ST	land_ice_mass
Ice mass not displacing seawater	kg	ST	land_ice_mass_not_displacing_sea_water
Area covered by grounded ice	m^2	ST	grounded_ice_sheet_area
Area covered by floating ice	m^2	ST	floating_ice_shelf_area
Total SMB flux	$kg\,s^{-1}$	FL	tendency_of_land_ice_mass_due_to_surface_mass_balance
Total BMB flux	$kg\,s^{-1}$	FL	tendency_of_land_ice_mass_due_to_basal_mass_balance
Total calving flux	$kg\,s^{-1}$	FL	tendency_of_land_ice_mass_due_to_calving

The Supplement related to this article is available online at https://doi.org/10.5194/tc-12-1433-2018-supplement.

Competing interests. The authors declare that they have no conflict of interest.

Acknowledgements. We acknowledge the Climate and Cryosphere (CliC) project and the World Climate Research Programme (WCRP) for their guidance, support, and sponsorship. We thank the CMIP6 panel members for their continuous leadership of the CMIP6 effort, and the Working Group on Coupled Modeling (WGCM) Infrastructure Panel (WIP) for overseeing the CMIP6 and ISMIP6 infrastructure and data request. We would like to thank Brice Noël for help with the SMB validation data and Xavier Fettweis, Miren Vizcaino, and Vincent Cabot for providing SMB data. We also thank Erika Simon for help with the data processing.

Andy Aschwanden, Eric Larour, Sophie Nowicki, and Helene Seroussi were supported by grants from the NASA Cryospheric Science Program and Modeling, Analysis, and Prediction Program. Heiko Goelzer has received funding from the programme of the Netherlands Earth System Science Centre (NESSC), financially supported by the Dutch Ministry of Education, Culture and Science (OCW) under grant no. 024.002.001. Nicholas R. Golledge is supported by Royal Society of New Zealand Rutherford Discovery Fellowship 15-VUW-004. Philippe Huybrechts acknowledges support from the iceMOD project funded by the Research Foundation – Flanders (FWO-Vlaanderen). William H. Lipscomb and Joseph H. Kennedy were supported by the Regional and Global Climate Modeling and Earth System Modeling programmes of the U.S. Department of Energy's Office of Science. The National Center for Atmospheric Research is sponsored by the National Science Foundation. Victoria Lee, Stephen L. Cornford, and Antony J. Payne carried out work as part of the UKESM contribution for CMIP6. Mathieu Morlighem was supported by NASA's Cryospheric Sciences Program (no. NNX15AD55G) and the National Science Foundation's Arctic System Science Program (ARCSS) (no. 1504230). Christian Rodehacke (DMI) has received funding from the European Research Council under the European Community's Seventh Framework Programme (FP7/2007–2013)/ERC grant agreement 610055 as part of the Ice2Ice project as well as the Nordic Center of Excellence eSTICC (eScience Tool for In-vestigating Climate Change in northern high latitudes) funded by Nordforsk (grant 57001). Florian A. Ziemen was supported by the BMBF project PALMOD. Computational resources for MPI-PISM were made available by DKRZ through support from BMBF. IGE-ELMER simulations were performed using the Froggy platform of the CIMENT infrastructure – which is supported by the Rhône-Alpes region (grant CPER07_13 CIRA), the OSUG@2020 laBex (reference ANR10 LABX56), and the Equip@Meso project (reference ANR-10-EQPX-29-01) – and using HPC resources from GENCI-CINES (grant 2016-016066). Ralf Greve, Ayako Abe-Ouchi, and Fuyuki Saito were supported by the Arctic Challenge for Sustainability (ArCS) project of the Japanese Ministry of Education, Culture, Sports, Science and Technology (MEXT), and by the Japan Society for the Promotion of Science (JSPS) KAKENHI under grant no. 17H06104, Ralf Greve and Ayako Abe-Ouchi were additionally supported under JSPS grant no. 16H02224, and Fuyuki Saito under JSPS grant no. 17K05664. Ayako Abe-Ouchi and Fuyuki Saito were supported by the Integrated Research Program for Advancing Climate Models (TOUGOU program) from MEXT. Reinhard Calov was funded by the Leibniz Association grant SAW-2014-PIK-1 and is now funded by the Bundesministerium für Bildung und Forschung (BMBF) grants PalMod-1.1-TP5 and PalMod-1.3-TP4.

Edited by: G. Hilmar Gudmundsson
Reviewed by: two anonymous referees

References

Adalgeirsdottir, G., Aschwanden, A., Khroulev, C., Boberg, F., Mottram, R., Lucas-Picher, P., and Christensen, J. H.: Role of model initialization for projections of 21st-century Greenland ice sheet mass loss, J. Glaciol., 60, 782–794, https://doi.org/10.3189/2014JoG13J202, 2014.

Alexander, P. M., Tedesco, M., Schlegel, N.-J., Luthcke, S. B., Fettweis, X., and Larour, E.: Greenland Ice Sheet seasonal and spatial mass variability from model simulations and GRACE (2003–2012), The Cryosphere, 10, 1259–1277, https://doi.org/10.5194/tc-10-1259-2016, 2016.

Andersen, K., Azuma, N., Barnola, J., Bigler, M., Biscaye, P., Caillon, N., Chappellaz, J., Clausen, H., DahlJensen, D., Fischer, H., Fluckiger, J., Fritzsche, D., Fujii, Y., Goto-Azuma, K., Gronvold, K., Gundestrup, N., Hansson, M., Huber, C., Hvidberg, C., Johnsen, S., Jonsell, U., Jouzel, J., Kipfstuhl, S., Landais, A., Leuenberger, M., Lorrain, R., Masson-Delmotte, V., Miller, H., Motoyama, H., Narita, H., Popp, T., Rasmussen, S., Raynaud, D., Rothlisberger, R., Ruth, U., Samyn, D., Schwander, J., Shoji, H., Siggard-Andersen, M., Steffensen, J., Stocker, T., Sveinbjornsdottir, A., Svensson, A., Takata, M., Tison, J., Thorsteinsson, T., Watanabe, O., Wilhelms, F., White, J., and Project, N. G. I. C.: High-resolution record of Northern Hemisphere climate extending into the last interglacial period, Nature, 431, 147–151, https://doi.org/10.1038/nature02805, 2004.

Arthern, R. and Gudmundsson, G.: Initialization of ice-sheet forecasts viewed as an inverse Robin problem, J. Glaciol., 56, 527–533, 2010.

Arthern, R. J., Hindmarsh, R. C. A., and Williams, C. R.: Flow speed within the Antarctic ice sheet and its controls inferred from satellite observations, J. Geophys. Res.-Earth, 120, 2014JF003239, https://doi.org/10.1002/2014JF003239, 2015.

Asay-Davis, X. S., Cornford, S. L., Durand, G., Galton-Fenzi, B. K., Gladstone, R. M., Gudmundsson, G. H., Hattermann, T., Holland, D. M., Holland, D., Holland, P. R., Martin, D. F., Mathiot, P., Pattyn, F., and Seroussi, H.: Experimental design for three interrelated marine ice sheet and ocean model intercomparison projects: MISMIP v. 3 (MISMIP+), ISOMIP v. 2 (ISOMIP +) and MISOMIP v. 1 (MISOMIP1), Geosci. Model Dev., 9, 2471–2497, https://doi.org/10.5194/gmd-9-2471-2016, 2016.

Aschwanden, A., Aðalgeirsdóttir, G., and Khroulev, C.: Hindcasting to measure ice sheet model sensitivity to initial states, The Cryosphere, 7, 1083–1093, https://doi.org/10.5194/tc-7-1083-2013, 2013.

Aschwanden, A., Fahnestock, M. A., and Truffer, M.: Complex Greenland outlet glacier flow captured, Nat. Commun., 7, 10524, https://doi.org/10.1038/ncomms10524, 2016.

Bales, R. C., Guo, Q., Shen, D., Mcconnell, J. R., Du, G., Burkhart, J. F., Spikes, V. B., Hanna, E., and Cappelen, J.: Annual accumulation for Greenland updated using ice core data developed during 2000–2006 and analysis of daily coastal meteorological data, J. Geophys. Res., 114, D06116, https://doi.org/10.1029/2008JD011208, 2009.

Bamber, J. L., Ekholm, S., and Krabill, W. B.: A new, high-resolution digital elevation model of Greenland fully validated with airborne laser altimeter data, J. Geophys. Res., 106, 6733–6745, 2001.

Bamber, J. L., Griggs, J. A., Hurkmans, R. T. W. L., Dowdeswell, J. A., Gogineni, S. P., Howat, I., Mouginot, J., Paden, J., Palmer, S., Rignot, E., and Steinhage, D.: A new bed elevation dataset for Greenland, The Cryosphere, 7, 499-510, https://doi.org/10.5194/tc-7-499-2013, 2013.

Barker, S., Knorr, G., Edwards, R. L., Parrenin, F., Putnam, A. E., Skinner, L. C., Wolff, E., and Ziegler, M.: 800,000 Years of Abrupt Climate Variability, Science, 334, 347–351, https://doi.org/10.1126/science.1203580, 2011.

Bindschadler, R. A., Nowicki, S., Abe-Ouchi, A., Aschwanden, A., Choi, H., Fastook, J., Granzow, G., Greve, R., Gutowski, G., Herzfeld, U., Jackson, C., Johnson, J., Khroulev, C., Levermann, A., Lipscomb, W. H., Martin, M. A., Morlighem, M., Parizek, B. R., Pollard, D., Price, S. F., Ren, D., Saito, F., Sato, T., Seddik, H., Seroussi, H., Takahashi, K., Walker, R., and Wang, W. L.: Ice-sheet model sensitivities to environmental forcing and their use in projecting future sea level (the SeaRISE project), J. Glaciol., 59, 195–224, https://doi.org/10.3189/2013JoG12J125, 2013.

Box, J.: Greenland Ice Sheet Mass Balance Reconstruction. Part II: Surface Mass Balance (1840–2010), J. Climate, 26, 6974–6989, https://doi.org/10.1175/jcli-d-12-00518.1, 2013.

Calov, R., Greve, R., Abe-Ouchi, A., Bueler, E., Huybrechts, P., Johnson, J., Pattyn, F., Pollard, D., Ritz, C., Saito, F., and Tarasov, L.: Results from the Ice-Sheet Model Intercomparison Project–Heinrich Event INtercOmparison (ISMIP HEINO), J. Glaciol., 56, 371–383, 2010.

Calov, R., Robinson, A., Perrette, M., and Ganopolski, A.: Simulating the Greenland ice sheet under present-day and palaeo constraints including a new discharge parameterization, The Cryosphere, 9, 179–196, https://doi.org/10.5194/tc-9-179-2015, 2015.

Dansgaard, W., Johnsen, S. J., Clausen, H. B., Dahl-Jensen, D., Gundestrup, N. S., Hammer, C. U., Hvidberg, C. S., Steffensen, J. P., Sveinbjoernsdottir, A. E., Jouzel, J., and Bond, G. C.: Evidence for general instability of past climate from a 250-kyr ice-core record, Nature, 364, 218–220, 1993.

de Boer, B., Stocchi, P., and van de Wal, R. S. W.: A fully coupled 3-D ice-sheet–sea-level model: algorithm and applications, Geosci. Model Dev., 7, 2141–2156, https://doi.org/10.5194/gmd-7-2141-2014, 2014.

Drewry, D. J., Morris, E. M., Robin, G. D. Q., and Weller, G.: The Response of Large Ice Sheets to Climatic Change, Philos. T. Roy. Soc. B, 338, 235–242, https://doi.org/10.1098/rstb.1992.0143, 1992.

Edwards, T. L., Fettweis, X., Gagliardini, O., Gillet-Chaulet, F., Goelzer, H., Gregory, J. M., Hoffman, M., Huybrechts, P., Payne, A. J., Perego, M., Price, S., Quiquet, A., and Ritz, C.: Probabilistic parameterisation of the surface mass balance–elevation feedback in regional climate model simulations of the Greenland ice sheet, The Cryosphere, 8, 181–194, https://doi.org/10.5194/tc-8-181-2014, 2014a.

Edwards, T. L., Fettweis, X., Gagliardini, O., Gillet-Chaulet, F., Goelzer, H., Gregory, J. M., Hoffman, M., Huybrechts, P., Payne, A. J., Perego, M., Price, S., Quiquet, A., and Ritz, C.: Effect of uncertainty in surface mass balance–elevation feedback on projections of the future sea level contribution of the Greenland ice sheet, The Cryosphere, 8, 195–208, https://doi.org/10.5194/tc-8-195-2014, 2014b.

Enderlin, E. M., Howat, I. M., Jeong, S., Noh, M.-J., van Angelen, J. H., and van den Broeke, M. R.: An improved mass budget for the Greenland ice sheet, Geophys. Res. Lett., 41, 2013GL059010, https://doi.org/10.1002/2013GL059010, 2014.

Ettema, J., Van Den Broeke, M. R., Van Meijgaard, E., Van De Berg, W. J., Bamber, J. L., Box, J. E., and Bales, R. C.: Higher surface mass balance of the Greenland ice sheet revealed by high-resolution climate modeling, Geophys. Res. Lett., 36, L12501, https://doi.org/10.1029/2009GL038110, 2009.

Eyring, V., Bony, S., Meehl, G. A., Senior, C. A., Stevens, B., Stouffer, R. J., and Taylor, K. E.: Overview of the Coupled Model Intercomparison Project Phase 6 (CMIP6) experimental design and organization, Geosci. Model Dev., 9, 1937–1958, https://doi.org/10.5194/gmd-9-1937-2016, 2016.

Fausto, R. S., Ahlstrøm, A. P., Van As, D., Bøggild, C. E., and Johnsen, S. J.: A new present-day temperature parameterization for Greenland, J. Glaciol., 55, 95–105, https://doi.org/10.3189/002214309788608985, 2009.

Fettweis, X., Box, J. E., Agosta, C., Amory, C., Kittel, C., Lang, C., van As, D., Machguth, H., and Gallée, H.: Reconstructions of the 1900–2015 Greenland ice sheet surface mass balance using the regional climate MAR model, The Cryosphere, 11, 1015–1033, https://doi.org/10.5194/tc-11-1015-2017, 2017.

Fox Maule, C., Purucker, M. E., Olsen, N., and Mosegaard, K.: Heat flux anomalies in Antarctica revealed by satellite magnetic data, Science, 309, 464–467, 2005.

Franco, B., Fettweis, X., Lang, C., and Erpicum, M.: Impact of spatial resolution on the modelling of the Greenland ice sheet surface mass balance between 1990–2010, using the regional climate model MAR, The Cryosphere, 6, 695–711, https://doi.org/10.5194/tc-6-695-2012, 2012.

Fürst, J. J., Goelzer, H., and Huybrechts, P.: Ice-dynamic projections of the Greenland ice sheet in response to atmospheric and oceanic warming, The Cryosphere, 9, 1039–1062, https://doi.org/10.5194/tc-9-1039-2015, 2015.

Gillet-Chaulet, F., Gagliardini, O., Seddik, H., Nodet, M., Durand, G., Ritz, C., Zwinger, T., Greve, R., and Vaughan, D. G.: Greenland ice sheet contribution to sea-level rise from a new-generation ice-sheet model, The Cryosphere, 6, 1561–1576, https://doi.org/10.5194/tc-6-1561-2012, 2012.

Goelzer, H., Huybrechts, P., Raper, S. C. B., Loutre, M.-F., Goosse, H., and Fichefet, T.: Millennial total sea-level commitments projected with the Earth system model of intermediate complexity LOVECLIM, Environ. Res. Lett., 7, 1–9, https://doi.org/10.1088/1748-9326/7/4/045401, 2012.

Goelzer, H., Huybrechts, P., Fürst, J. J., Andersen, M. L., Edwards, T. L., Fettweis, X., Nick, F. M., Payne, A. J.,

and Shannon, S. R.: Sensitivity of Greenland ice sheet projections to model formulations, J. Glaciol., 59, 733–749, https://doi.org/10.3189/2013JoG12J182, 2013.

Goelzer, H., Robinson, A., Seroussi, H., and Van De Wal, R. S. W.: Recent Progress in Greenland Ice Sheet Modelling, Current Climate Change Reports, 3, 291–302, https://doi.org/10.1007/s40641-017-0073-y, 2017.

Goldberg, D. N. and Heimbach, P.: Parameter and state estimation with a time-dependent adjoint marine ice sheet model, The Cryosphere, 7, 1659–1678, https://doi.org/10.5194/tc-7-1659-2013, 2013.

Golledge, N. R., Menviel, L., Carter, L., Fogwill, C. J., England, M. H., Cortese, G., and Levy, R. H.: Antarctic contribution to meltwater pulse 1A from reduced Southern Ocean overturning, Nat. Commun., 5, 5107, https://doi.org/10.1038/ncomms6107, 2014.

Golledge, N. R., Kowalewski, D. E., Naish, T. R., Levy, R. H., Fogwill, C. J., and Gasson, E. G. W.: The multi-millennial Antarctic commitment to future sea-level rise, Nature, 526, 421–425, https://doi.org/10.1038/nature15706, 2015.

Greve, R.: Relation of measured basal temperatures and the spatial distribution of the geothermal heat flux for the Greenland ice sheet, Ann. Glaciol., 42, 424–432, https://doi.org/10.3189/172756405781812510, 2005.

Greve, R. and Blatter, H.: Comparison of thermodynamics solvers in the polythermal ice sheet model SICOPOLIS, Polar Sci., 10, 11–23, https://doi.org/10.1016/j.polar.2015.12.004, 2016.

Greve, R. and Herzfeld, U. C.: Resolution of ice streams and outlet glaciers in large-scale simulations of the Greenland ice sheet, Ann. Glaciol., 54, 209–220, https://doi.org/10.3189/2013AoG63A085, 2013.

Greve, R., Saito, F., and Abe-Ouchi, A.: Initial results of the SeaRISE numerical experiments with the models SICOPOLIS and IcIES for the Greenland ice sheet, Ann. Glaciol., 52, 23–30, 2011.

Helsen, M. M., van de Wal, R. S. W., van den Broeke, M. R., van de Berg, W. J., and Oerlemans, J.: Coupling of climate models and ice sheet models by surface mass balance gradients: application to the Greenland Ice Sheet, The Cryosphere, 6, 255–272, https://doi.org/10.5194/tc-6-255-2012, 2012.

Herzfeld, U. C., McDonald, B. W., Wallin, B. F., Chen, P. A., Mayer, H., Paden, J., and Leuschen, C. J.: The trough-system algorithm and its application to spatial modeling of Greenland subglacial topography, Ann. Glaciol., 55, 115–126, https://doi.org/10.3189/2014AoG67A001, 2014.

Hindmarsh, R. C. A. and Le Meur, E.: Dynamical processes involved in the retreat of marine ice sheets, J. Glaciol., 47, 271–282, https://doi.org/10.3189/172756501781832269, 2001.

Howat, I. M., Negrete, A., and Smith, B. E.: The Greenland Ice Mapping Project (GIMP) land classification and surface elevation data sets, The Cryosphere, 8, 1509–1518, https://doi.org/10.5194/tc-8-1509-2014, 2014.

Huybrechts, P.: Sea-level changes at the LGM from ice-dynamic reconstructions of the Greenland and Antarctic ice sheets during the glacial cycles, Quaternary Sci. Rev., 21, 203–231, https://doi.org/10.1016/S0277-3791(01)00082-8, 2002.

Huybrechts, P. and de Wolde, J.: The dynamic response of the Greenland and Antarctic ice sheets to multiple-century climatic warming, J. Climate, 12, 2169–2188, https://doi.org/10.1175/1520-0442(1999)012<2169:TDROTG>2.0.CO;2, 1999.

Huybrechts, P., Letréguilly, A., and Reeh, N.: The Greenland ice sheet and greenhouse warming, Global Planet. Change, 3, 399–412, 1991.

Huybrechts, P., Payne, A. J., and Group, E. I.: The EISMINT benchmarks for testing ice-sheet models, Ann. Glaciol., 23, 1–12, 1996.

Huybrechts, P., Janssens, I., Poncin, C., and Fichefet, T.: The response of the Greenland ice sheet to climate changes in the 21st century by interactive coupling of an AOGCM with a thermomechanical ice-sheet model, Ann. Glaciol., 35, 409–415, 2002.

Imbrie, J., Boyle, E. A., Clemens, S. C., Duffy, A., Howard, W. R., Kukla, G., Kutzbach, J., Martinson, D. G., McIntyre, A., Mix, A. C., Molfino, B., Morley, J. J., Peterson, L. C., Pisias, N. G., Prell, W. L., Raymo, M. E., Shackleton, N. J., and Toggweiler, J. R.: On the Structure and Origin of Major Glaciation Cycles 1. Linear Responses to Milankovitch Forcing, Paleoceanography, 7, 701–738, https://doi.org/10.1029/92PA02253, 1992.

Johnsen, S. J., Clausen, H. B., Dansgaard, W., Gundestrup, N. S., Hammer, C. U., Andersen, U., Andersen, K. K., Hvidberg, C. S., Dahl-Jensen, D., Steffensen, J. P., Shoji, H., Sveinbjörnsdóttir, Á. E., White, J., Jouzel, J., and Fisher, D.: The δ18O record along the Greenland Ice Core Project deep ice core and the problem of possible Eemian climatic instability, J. Geophys. Res.-Oceans, 102, 26397–26410, https://doi.org/10.1029/97JC00167, 1997.

Jones, P. W.: First- and Second-Order Conservative Remapping Schemes for Grids in Spherical Coordinates, Mon. Weather Rev., 127, 2204–2210, https://doi.org/10.1175/1520-0493(1999)127<2204:fasocr>2.0.co;2, 1999.

Joughin, I., Smith, B., Howat, I., and Scambos, T.: MEaSUREs Greenland Ice Sheet Velocity Map from InSAR Data, Version 1., Boulder, Colorado USA, NASA National Snow and Ice Data Center Distributed Active Archive Center, https://doi.org/10.5067/MEASURES/CRYOSPHERE/nsidc-0478.001, 2010a.

Joughin, I., Smith, B., Howat, I. M., Scambos, T., and Moon, T.: Greenland flow variability from ice-sheet-wide velocity mapping, J. Glaciol., 56, 415–430, https://doi.org/10.3189/002214310792447734, 2010b.

Joughin, I., Smith, B., Howat, I., and Scambos, T.: MEaSUREs Multi-year Greenland Ice Sheet Velocity Mosaic, Version 1., Boulder, Colorado USA, NASA National Snow and Ice Data Center Distributed Active Archive Center, https://doi.org/10.5067/QUA5Q9SVMSJG, 2016.

Kobashi, T., Kawamura, K., Severinghaus, J. P., Barnola, J.-M., Nakaegawa, T., Vinther, B. M., Johnsen, S. J., and Box, J. E.: High variability of Greenland surface temperature over the past 4000 years estimated from trapped air in an ice core, Geophys. Res. Lett., 38, L21501, https://doi.org/10.1029/2011GL049444, 2011.

Larour, E., Seroussi, H., Morlighem, M., and Rignot, E.: Continental scale, high order, high spatial resolution, ice sheet modeling using the Ice Sheet System Model (ISSM), J. Geophys. Res., 117, F01022, https://doi.org/10.1029/2011JF002140, 2012.

Larour, E., Utke, J., Csatho, B., Schenk, A., Seroussi, H., Morlighem, M., Rignot, E., Schlegel, N., and Khazendar, A.: Inferred basal friction and surface mass balance of the Northeast Greenland Ice Stream using data assimilation of ICESat

(Ice Cloud and land Elevation Satellite) surface altimetry and ISSM (Ice Sheet System Model), The Cryosphere, 8, 2335–2351, https://doi.org/10.5194/tc-8-2335-2014, 2014.

Larour, E., Utke, J., Bovin, A., Morlighem, M., and Perez, G.: An approach to computing discrete adjoints for MPI-parallelized models applied to Ice Sheet System Model 4.11, Geosci. Model Dev., 9, 3907–3918, https://doi.org/10.5194/gmd-9-3907-2016, 2016.

Lee, V., Cornford, S. L., and Payne, A. J.: Initialization of an ice-sheet model for present-day Greenland, Ann. Glaciol., 56, 129–140, https://doi.org/10.3189/2015AoG70A121, 2015.

Lucas-Picher, P., Wulff-Nielsen, M., Christensen, J. H., Aðalgeirsdóttir, G., Mottram, R., and Simonsen, S. B.: Very high resolution regional climate model simulations over Greenland: Identifying added value, J. Geophys. Res.-Atmos., 117, D02108, https://doi.org/10.1029/2011JD016267, 2012.

Machguth, H., Thomsen, H. H., Weidick, A., Ahlstrøm, A. P., Abermann, J., Andersen, M. L., Andersen, S. B., Bjørk, A. A., Box, J. E., Braithwaite, R. J., Bøggild, C. E., Citterio, M., Clement, P., Colgan, W., Fausto, R. S., Gleie, K., Gubler, S., Hasholt, B., Hynek, B., Knudsen, N. T., Larsen, S. H., Mernild, S. H., Oerlemans, J., Oerter, H., Olesen, O. B., Smeets, C. J. P. P., Steffen, K., Stober, M., Sugiyama, S., Van As, D., Van Den Broeke, M. R., and Van De Wal, R. S. W.: Greenland surface mass-balance observations from the ice-sheet ablation area and local glaciers, J. Glaciol., 62, 861–887, https://doi.org/10.1017/jog.2016.75, 2016.

MacGregor, J. A., Fahnestock, M. A., Catania, G. A., Paden, J. D., Prasad Gogineni, S., Young, S. K., Rybarski, S. C., Mabrey, A. N., Wagman, B. M., and Morlighem, M.: Radiostratigraphy and age structure of the Greenland Ice Sheet, J. Geophys. Res.-Earth, 120, 212–241, https://doi.org/10.1002/2014JF003215, 2015.

Morlighem, M., Rignot, E., Seroussi, H., Larour, E., Ben Dhia, H., and Aubry, D.: Spatial patterns of basal drag inferred using control methods from a full-Stokes and simpler models for Pine Island Glacier, West Antarctica, Geophys. Res. Lett., 37, L14502, https://doi.org/10.1029/2010GL043853, 2010.

Morlighem, M., Rignot, E., Seroussi, H., Larour, E., Ben Dhia, H., and Aubry, D.: A mass conservation approach for mapping glacier ice thickness, Geophys. Res. Lett., 38, L19503, https://doi.org/10.1029/2011GL048659, 2011.

Morlighem, M., Rignot, E., Mouginot, J., Seroussi, H., and Larour, E.: Deeply incised submarine glacial valleys beneath the Greenland ice sheet, Nat. Geosci., 7, 418–422, https://doi.org/10.1038/ngeo2167, 2014.

Morlighem, M., Rignot, E., Mouginot, J., Seroussi, H., and Larour, E.: IceBridge BedMachine Greenland, Version 2., Boulder, Colorado USA, NASA National Snow and Ice Data Center Distributed Active Archive Center, https://doi.org/10.5067/AD7B0HQNSJ29, 2015.

Morlighem, M., Williams, C. N., Rignot, E., An, L., Arndt, J. E., Bamber, J. L., Catania, G., Chauché, N., Dowdeswell, J. A., Dorschel, B., Fenty, I., Hogan, K., Howat, I., Hubbard, A., Jakobsson, M., Jordan, T. M., Kjeldsen, K. K., Millan, R., Mayer, L., Mouginot, J., Noël, B. P. Y., Cofaigh, C. Ó., Palmer, S., Rysgaard, S., Seroussi, H., Siegert, M. J., Slabon, P., Straneo, F., van den Broeke, M. R., Weinrebe, W., Wood, M., and Zinglersen, K. B.: BedMachine v3: Complete bed topography and ocean bathymetry mapping of Greenland from multi-beam echo sounding combined with mass conservation, Geophys. Res. Lett., 44, 11051–11061, https://doi.org/10.1002/2017GL074954, 2017.

Mosbeux, C., Gillet-Chaulet, F., and Gagliardini, O.: Comparison of adjoint and nudging methods to initialise ice sheet model basal conditions, Geosci. Model Dev., 9, 2549–2562, https://doi.org/10.5194/gmd-9-2549-2016, 2016.

Mouginot, J., Rignot, E., Scheuchl, B., Fenty, I., Khazendar, A., Morlighem, M., Buzzi, A., and Paden, J.: Fast retreat of Zachariæ Isstrøm, northeast Greenland, Science, 350, 1357–1361, https://doi.org/10.1126/science.aac7111, 2015.

Nick, F. M., Vieli, A., Andersen, M. L., Joughin, I., Payne, A., Edwards, T. L., Pattyn, F., and van de Wal, R. S. W.: Future sea-level rise from Greenland/'s main outlet glaciers in a warming climate, Nature, 497, 235–238, https://doi.org/10.1038/nature12068, 2013.

Noël, B., van de Berg, W. J., Machguth, H., Lhermitte, S., Howat, I., Fettweis, X., and van den Broeke, M. R.: A daily, 1 km resolution data set of downscaled Greenland ice sheet surface mass balance (1958–2015), The Cryosphere, 10, 2361–2377, https://doi.org/10.5194/tc-10-2361-2016, 2016.

Nowicki, S., Bindschadler, R. A., Abe-Ouchi, A., Aschwanden, A., Bueler, E., Choi, H., Fastook, J., Granzow, G., Greve, R., Gutowski, G., Herzfeld, U., Jackson, C., Johnson, J., Khroulev, C., Larour, E., Levermann, A., Lipscomb, W. H., Martin, M. A., Morlighem, M., Parizek, B. R., Pollard, D., Price, S. F., Ren, D., Rignot, E., Saito, F., Sato, T., Seddik, H., Seroussi, H., Takahashi, K., Walker, R., and Wang, W. L.: Insights into spatial sensitivities of ice mass response to environmental change from the SeaRISE ice sheet modeling project II: Greenland, J. Geophys. Res.-Earth, 118, 1025–1044, https://doi.org/10.1002/jgrf.20076, 2013a.

Nowicki, S., Bindschadler, R. A., Abe-Ouchi, A., Aschwanden, A., Bueler, E., Choi, H., Fastook, J., Granzow, G., Greve, R., Gutowski, G., Herzfeld, U., Jackson, C., Johnson, J., Khroulev, C., Larour, E., Levermann, A., Lipscomb, W. H., Martin, M. A., Morlighem, M., Parizek, B. R., Pollard, D., Price, S. F., Ren, D., Rignot, E., Saito, F., Sato, T., Seddik, H., Seroussi, H., Takahashi, K., Walker, R., and Wang, W. L.: Insights into spatial sensitivities of ice mass response to environmental change from the SeaRISE ice sheet modeling project I: Antarctica, J. Geophys. Res.-Earth, 118, 1002–1024, https://doi.org/10.1002/jgrf.20081, 2013b.

Nowicki, S. M. J., Payne, A., Larour, E., Seroussi, H., Goelzer, H., Lipscomb, W., Gregory, J., Abe-Ouchi, A., and Shepherd, A.: Ice Sheet Model Intercomparison Project (ISMIP6) contribution to CMIP6, Geosci. Model Dev., 9, 4521–4545, https://doi.org/10.5194/gmd-9-4521-2016, 2016.

Pattyn, F.: Sea-level response to melting of Antarctic ice shelves on multi-centennial timescales with the fast Elementary Thermomechanical Ice Sheet model (f.ETISh v1.0), The Cryosphere, 11, 1851–1878, https://doi.org/10.5194/tc-11-1851-2017, 2017.

Pattyn, F., Perichon, L., Aschwanden, A., Breuer, B., de Smedt, B., Gagliardini, O., Gudmundsson, G. H., Hindmarsh, R. C. A., Hubbard, A., Johnson, J. V., Kleiner, T., Konovalov, Y., Martin, C., Payne, A. J., Pollard, D., Price, S., Rückamp, M., Saito, F., Soucek, O., Sugiyama, S., and Zwinger, T.: Benchmark experiments for higher-order and full-Stokes ice sheet models (ISMIP–HOM), The Cryosphere, 2, 95–108, https://doi.org/10.5194/tc-2-95-2008, 2008.

Pattyn, F., Schoof, C., Perichon, L., Hindmarsh, R. C. A., Bueler, E., de Fleurian, B., Durand, G., Gagliardini, O., Gladstone,

R., Goldberg, D., Gudmundsson, G. H., Huybrechts, P., Lee, V., Nick, F. M., Payne, A. J., Pollard, D., Rybak, O., Saito, F., and Vieli, A.: Results of the Marine Ice Sheet Model Intercomparison Project, MISMIP, The Cryosphere, 6, 573–588, https://doi.org/10.5194/tc-6-573-2012, 2012.

Pattyn, F., Perichon, L., Durand, G., Favier, L., Gagliardini, O., Hindmarsh, R. C. A., Zwinger, T., Albrecht, T., Cornford, S., Docquier, D., Fürst, J. J., Goldberg, D., Gudmundsson, G. H., Humbert, A., Hütten, M., Huybrechts, P., Jouvet, G., Kleiner, T., Larour, E., Martin, D., Morlighem, M., Payne, A. J., Pollard, D., Rückamp, M., Rybak, O., Seroussi, H., Thoma, M., and Wilkens, N.: Grounding-line migration in plan-view marine ice-sheet models: results of the ice2sea MISMIP3d intercomparison, J. Glaciol., 59, 410–422, https://doi.org/10.3189/2013JoG12J129, 2013.

Payne, A. J., Huybrechts, P., Abe-Ouchi, A., Calov, R., Fastook, J. L., Greve, R., Marshall, S. J., Marsiat, I., Ritz, C., Tarasov, L., and Thomassen, M. P. A.: Results from the EISMINT Phase 2 simplified geometry experiments: the effects of thermomechanical coupling, J. Glaciol., 46, 227–238, 2000.

Perego, M., Price, S., and Stadler, G.: Optimal initial conditions for coupling ice sheet models to Earth system models, J. Geophys. Res.-Earth, 119, 1894–1917, https://doi.org/10.1002/2014jf003181, 2014.

Pollard, D. and DeConto, R. M.: Description of a hybrid ice sheet-shelf model, and application to Antarctica, Geosci. Model Dev., 5, 1273–1295, https://doi.org/10.5194/gmd-5-1273-2012, 2012a.

Pollard, D. and DeConto, R. M.: A simple inverse method for the distribution of basal sliding coefficients under ice sheets, applied to Antarctica, The Cryosphere, 6, 953–971, https://doi.org/10.5194/tc-6-953-2012, 2012b.

Price, S. F., Payne, A. J., Howat, I. M., and Smith, B. E.: Committed sea-level rise for the next century from Greenland ice sheet dynamics during the past decade, P. Natl. Acad. Sci. USA, 108, 8978–8983, https://doi.org/10.1073/pnas.1017313108, 2011.

Price, S. F., Hoffman, M. J., Bonin, J. A., Howat, I. M., Neumann, T., Saba, J., Tezaur, I., Guerber, J., Chambers, D. P., Evans, K. J., Kennedy, J. H., Lenaerts, J., Lipscomb, W. H., Perego, M., Salinger, A. G., Tuminaro, R. S., van den Broeke, M. R., and Nowicki, S. M. J.: An ice sheet model validation framework for the Greenland ice sheet, Geosci. Model Dev., 10, 255–270, https://doi.org/10.5194/gmd-10-255-2017, 2017.

Rastner, P., Bolch, T., Mölg, N., Machguth, H., Le Bris, R., and Paul, F.: The first complete inventory of the local glaciers and ice caps on Greenland, The Cryosphere, 6, 1483–1495, https://doi.org/10.5194/tc-6-1483-2012, 2012.

Rignot, E. and Mouginot, J.: Ice flow in Greenland for the International Polar Year 2008–2009, Geophys. Res. Lett., 39, L11501, https://doi.org/10.1029/2012GL051634, 2012.

Robinson, A., Calov, R., and Ganopolski, A.: An efficient regional energy-moisture balance model for simulation of the Greenland Ice Sheet response to climate change, The Cryosphere, 4, 129–144, https://doi.org/10.5194/tc-4-129-2010, 2010.

Saito, F., Abe-Ouchi, A., Takahashi, K., and Blatter, H.: SeaRISE experiments revisited: potential sources of spread in multi-model projections of the Greenland ice sheet, The Cryosphere, 10, 43–63, https://doi.org/10.5194/tc-10-43-2016, 2016.

Schlegel, N. J., Larour, E., Seroussi, H., Morlighem, M., and Box, J. E.: Decadal-scale sensitivity of Northeast Greenland ice flow to errors in surface mass balance using ISSM, J. Geophys. Res.-Earth, 118, 667–680, https://doi.org/10.1002/jgrf.20062, 2013.

Schlegel, N.-J., Wiese, D. N., Larour, E. Y., Watkins, M. M., Box, J. E., Fettweis, X., and van den Broeke, M. R.: Application of GRACE to the assessment of model-based estimates of monthly Greenland Ice Sheet mass balance (2003–2012), The Cryosphere, 10, 1965–1989, https://doi.org/10.5194/tc-10-1965-2016, 2016.

Schoof, C.: Ice sheet grounding line dynamics: Steady states, stability, and hysteresis, J. Geophys. Res., 112, F03S28, https://doi.org/10.1029/2006JF000664, 2007.

Seroussi, H., Morlighem, M., Rignot, E., Larour, E., Aubry, D., Ben Dhia, H., and Kristensen, S. S.: Ice flux divergence anomalies on 79 north Glacier, Greenland, Geophys. Res. Lett., 38, L09501, https://doi.org/10.1029/2011GL047338, 2011.

Seroussi, H., Morlighem, M., Rignot, E., Khazendar, A., Larour, E., and Mouginot, J.: Dependence of century-scale projections of the Greenland ice sheet on its thermal regime, J. Glaciol., 59, 1024–1034, https://doi.org/10.3189/2013JoG13J054, 2013.

Seroussi, H., Morlighem, M., Larour, E., Rignot, E., and Khazendar, A.: Hydrostatic grounding line parameterization in ice sheet models, The Cryosphere, 8, 2075–2087, https://doi.org/10.5194/tc-8-2075-2014, 2014.

Shannon, S. R., Payne, A. J., Bartholomew, I. D., van den Broeke, M. R., Edwards, T. L., Fettweis, X., Gagliardini, O., Gillet-Chaulet, F., Goelzer, H., Hoffman, M. J., Huybrechts, P., Mair, D., Nienow, P., Perego, M., Price, S. F., Smeets, C. J. P. P., Sole, A. J., van de Wal, R. S. W., and Zwinger, T.: Enhanced basal lubrication and the contribution of the Greenland ice sheet to future sea level rise, P. Natl. Acad. Sci. USA, 110, 14156–14161, https://doi.org/10.1073/pnas.1212647110, 2013.

Shapiro, N. M. and Ritzwoller, M. H.: Inferring surface heat flux distributions guided by a global seismic model: particular application to Antarctica, Earth Planet. Sc. Lett., 223, 213–224, https://doi.org/10.1016/j.epsl.2004.04.011, 2004.

Snyder, J.: Map projections – a working manual (USGS Professional Paper 1395), United States Government Printing Office, Washington, USA, 1987.

Svendsen, S. H., Madsen, M. S., Yang, S., Rodehacke, C., and Adalgeirsdottir, G.: An Introduction to the Coupled EC-Earth-PISM Model System, Danish Meteorological Institute, Copenhagen, Denmark, 2015.

Svensson, A., Andersen, K. K., Bigler, M., Clausen, H. B., Dahl-Jensen, D., Davies, S. M., Johnsen, S. J., Muscheler, R., Parrenin, F., Rasmussen, S. O., Röthlisberger, R., Seierstad, I., Steffensen, J. P., and Vinther, B. M.: A 60 000 year Greenland stratigraphic ice core chronology, Clim. Past, 4, 47–57, https://doi.org/10.5194/cp-4-47-2008, 2008.

Taylor, A. D.: A model of iceberg calving in Greenland, PhD Thesis, University of Bristol, Bristol, UK, 271 pp., 2016.

van Angelen, J. H., van den Broeke, M. R., Wouters, B., and Lenaerts, J. T. M.: Contemporary (1960–2012) Evolution of the Climate and Surface Mass Balance of the Greenland Ice Sheet, Surv. Geophys., 35, 1155–1174, https://doi.org/10.1007/s10712-013-9261-z, 2014.

van den Broeke, M., Bamber, J., Ettema, J., Rignot, E., Schrama, E., van de Berg, W. J., van Meijgaard, E., Velicogna, I., and Wouters, B.: Partitioning Recent Greenland Mass Loss, Science, 326, 984–986, https://doi.org/10.1126/science.1178176, 2009.

Velicogna, I., Sutterley, T. C., and van den Broeke, M. R.: Regional acceleration in ice mass loss from Greenland and Antarctica using GRACE time-variable gravity data, Geophys. Res. Lett., 41, 8130–8137, https://doi.org/10.1002/2014GL061052, 2014.

Vizcaino, M., Mikolajewicz, U., Ziemen, F., Rodehacke, C. B., Greve, R., and van den Broeke, M. R.: Coupled simulations of Greenland Ice Sheet and climate change up to A.D. 2300, Geophys. Res. Lett., 42, 3927–3935, https://doi.org/10.1002/2014GL061142, 2015.